Evolution of Cardiac Calcium Waves from Stochastic Calcium Sparks

Leighton T. Izu,* W. Gil Wier,† and C. William Balke*†
Departments of *Medicine and †Physiology, University of Maryland School of Medicine, Baltimore, Maryland 21201 USA

ABSTRACT We present a model that provides a unified framework for studying Ca^{2+} sparks and Ca^{2+} waves in cardiac cells. The model is novel in combining 1) use of large currents (~20 pA) through the Ca^{2+} release units (CRUs) of the sarcoplasmic reticulum (SR); 2) stochastic Ca^{2+} release (or firing) of CRUs; 3) discrete, asymmetric distribution of CRUs along the longitudinal (separation distance of 2 μm) and transverse (separated by 0.4–0.8 μm) directions of the cell; and 4) anisotropic diffusion of Ca^{2+} and fluorescent indicator to study the evolution of Ca^{2+} waves from Ca^{2+} sparks. The model mimics the important features of Ca^{2+} sparks and Ca^{2+} waves in terms of the spontaneous spark rate, the Ca^{2+} wave velocity, and the pattern of wave propagation. Importantly, these features are reproduced when using experimentally measured values for the CRU Ca^{2+} sensitivity (~15 μM). Stochastic control of CRU firing is important because it imposes constraints on the Ca^{2+} sensitivity of the CRU. Even with moderate (~5 μM) Ca^{2+} sensitivity the very high spontaneous spark rate triggers numerous Ca^{2+} waves. In contrast, a single Ca^{2+} wave with arbitrarily large velocity can exist in a deterministic model when the CRU Ca^{2+} sensitivity is sufficiently high. The combination of low CRU Ca^{2+} sensitivity (~15 μM), high cytosolic Ca^{2+} buffering capacity, and the spatial separation of CRUs help control the inherent instability of SR Ca^{2+} release. This allows Ca^{2+} waves to form and propagate given a sufficiently large initiation region, but prevents a single spark or a small group of sparks from triggering a wave.

GLOSSARY

Most symbols were defined in the companion paper (Izu et al., 2001). Here we list new symbols and those that occur frequently in this paper.

x, y	spatial coordinates (μm)
t	time coordinate (ms)
C	free Ca^{2+} concentration (μM)
D_{Cx}, D_{Cy}	Ca^{2+} diffusion coefficients along x and y (μm^2/ms)
S	stochastic switching function equaling either 0 or 1
P_{max}	maximum probability of Ca^{2+} spark occurrence/calcium release unit/ms
P	probability of Ca^{2+} spark occurrence/calcium release unit/ms
n	Hill coefficient in definition of P
K	Ca^{2+} sensitivity parameter in definition of P (μM)
ℓ_x, ℓ_y	spatial separation of Ca^{2+} release units (CRUs) along x and y (μm)
σ	molar flux of CRU for 2-dimensional diffusion domains (pmol/ms/μm)
I_{SR}	current through the CRU (pA)
T_{open}	duration of current flow through CRU (ms)
C_0	baseline Ca^{2+} concentration (μM)
φ	waiting time distribution
$p(t < \tau)$	probability of a CRU not firing in time $t < \tau$
$P(X \geq 1, t < \tau)$	probability of at least one CRU firing in time $t < \tau$

Received for publication 24 May 2000 and in final form 16 October 2000.

Address reprint requests to Leighton T. Izu, University of Maryland School of Medicine, Department of Medicine Division of Cardiology, 22 South Green St., Baltimore, MD 21201-1595. Tel.: 410-706-2675; Fax: 410-706-8610; E-mail: lizu@umaryland.edu.

0006-3495/01/01/103/18 $2.00

INTRODUCTION

Slowly (~100 μm/s) propagating waves of elevated Ca^{2+} concentration (Ca^{2+} waves) appear to be a ubiquitous finding and have been observed in a wide diversity of cell types including skeletal (Endo, et al., 1970) and cardiac muscle (Fabiato and Fabiato, 1972), medaka eggs (Ridgway, et al., 1977), and astrocytes (Cornell-Bell and Finkbeiner, 1991). In cardiac atrial cells that lack transverse tubules (T tubules), physiological activation of the myofibrils in the interior of the cell depends on the propagation of a Ca^{2+} wave from the sarcolemma to the cell's center (Berlin, 1995; Hüser et al., 1996). In cardiac ventricle cells, Ca^{2+} waves are not physiological and are believed to be a pathological manifestation of Ca^{2+} overload and might trigger ventricular arrhythmias (Lakatta and Guarnieri, 1993).

Ca^{2+} waves are a natural consequence of regenerative Ca^{2+} release by the sarcoplasmic reticulum or Ca^{2+}-induced Ca^{2+}-release (CICR) (Endo, et al., 1970; Ford and Podolsky, 1970). All models of Ca^{2+} waves in skeletal and cardiac muscle have CICR at their core and the evolution of Ca^{2+} wave models reflects the growth of knowledge of excitation–contraction coupling in muscle. For example, an early mathematical model of Ca^{2+} waves (Backx et al., 1989) distributed Ca^{2+} release sites uniformly throughout the cytoplasm. However, in normal muscle cells, Ca^{2+} release sites are distributed in discrete bands at the z-lines (Carl, 1995). With the discovery of Ca^{2+} sparks (Cheng et al., 1993) the discrete nature of Ca^{2+} release was resolved to the opening of a few ryanodine receptors (RyRs) on the z-line in cardiac muscle (Shacklock et al., 1995). In addi-

tion, Cheng et al. (1993, 1996), speculated that Ca^{2+} waves arise from the collective firing of Ca^{2+} sparks.

Contemporary models of Ca^{2+} sparks and Ca^{2+} waves restrict Ca^{2+} release to the *z*-lines (Keizer et al., 1998; Keizer and Smith, 1998; Izu et al., 1999; Lukyanenko et al., 1999). However, understanding the relationship between Ca^{2+} sparks and Ca^{2+} waves in living cells has been complicated by asymmetries in cell structure, asymmetries in the Ca^{2+} spark profile, anisotropic diffusion of the Ca^{2+}-bound fluo-3, uncertainties regarding the Ca^{2+} sensitivity of the Ca^{2+} release units (CRU), and the Ca^{2+} currents required to generate Ca^{2+} sparks.

In this paper, we present a model that provides a unified framework for studying both Ca^{2+} sparks and Ca^{2+} waves. The following are key elements in this model.

1. Large CRU currents. By using relatively large CRU currents (5–20 pA; Izu et al., 2001) the model generates realistic Ca^{2+} sparks and realistic Ca^{2+} waves while maintaining CRU Ca^{2+}-sensitivities compatible with experimental measurements (Lukyanenko and Györke, 1999).
2. Stochastic triggering of Ca^{2+} release. Previous models of Ca^{2+} waves (except Keizer and Smith, 1998) have used a deterministic rule for triggering Ca^{2+} release; release occurred when the Ca^{2+} concentration exceeded some fixed value C^*. The use of stochastic instead of deterministic dynamics is important for two reasons. First, sparks occur spontaneously and randomly (Cheng et al., 1993) so a unified framework for studying sparks and waves must provide for the stochastic firing of the CRUs. Second, deterministic and stochastic systems can behave very differently when the Ca^{2+} sensitivity of the CRUs is high. In a deterministic system, waves can occur even when the sensitivity is arbitrarily high. However, in a stochastic system, even with moderately high CRU Ca^{2+} sensitivity ($\sim$5 μM), the large number of spontaneous sparks would trigger so many Ca^{2+} waves at once that observing a well-defined wave would be almost impossible.
3. Asymmetric distribution of discrete CRUs, and
4. anisotropic diffusion of Ca^{2+} and of mobile buffers. An important difference between our model and that of Keizer and coworkers (Keizer et al., 1998; Keizer and Smith, 1998) is how the Ca^{2+} buffers (endogenous and Ca^{2+} indicator) are handled. The Keizer models do not include buffers, and they compensate for the absence of buffers by reducing the free Ca^{2+} diffusion coefficient $\sim$10 fold. We will show that buffers endow the system with a property we call "superadditivity" that has profound effects on Ca^{2+} signaling, which extend much further than simply slowing Ca^{2+} diffusion.

The effect of three of the four key features in this model on Ca^{2+} wave propagation has been investigated by others. The effect of discrete, asymmetric distribution of CRUs was studied by Bugrim et al. (1997) and anisotropic Ca^{2+} diffusion was addressed by Kargacin and Fay (1991) and Girard et al. (1992). Keizer and Smith (1998) examined the effect of stochastic firing of CRUs on wave propagation. What is novel in our model is the combination of large CRU currents, stochastic triggering of CRU release, asymmetric distribution of CRUs, and anisotropic diffusion.

METHODS

Figure 1 shows the geometry of our model. *A* is the 3-dimensional (3D) schematic of a ventricular cell. The *x*-direction is the cell's longitudinal axis. The three vertical planes occur at the *z*-lines and are spaced a distance ℓ_x (=2 μm) apart. The black dots in the *y*–*z* plane are the CRUs. The horizontal plane is the 2-dimensional (2D) slice on which we will carry out our simulations. At present, we cannot do a full 3D simulation because of limitations in computational power. Figure 1 *B* shows CRUs in a *y*–*z* plane. Ca^{2+} release by discrete CRUs will generate concentration gradients in all directions. To eliminate gradients along *z*, the discrete CRUs along *z* are replaced by line sources that extend from $-\infty < z < \infty$ and spaced a distance of ℓ_y (0.4 or 0.8 μm) along *y* as shown in Fig. 1 *C*. These infinite line sources induce symmetry in *z* making planes at any *z* equivalent, thereby reducing the problem from three to two dimensions. Figure 1 *D* shows the plane on which the model is defined. The line sources intersect the *x*–*y* plane and at regular intervals of ℓ_x along *x* and ℓ_y along *y*. These intersections are called lattice sites.

The model equations are the same as Eqs. 2–7 in Izu et al. (2001), that describe the so-called "Smith buffer model." Apart from the restriction to two spatial dimensions, the only difference here is the differential equation for the free Ca^{2+} concentration $C(x, y, t)$ that is now

$$\frac{\partial C(x, y, t)}{\partial t} = D_{Cx}\frac{\partial^2 C}{\partial x^2} + D_{Cy}\frac{\partial^2 C}{\partial y^2} + R_B(C, F_B) + R_D(C, F_D) - J_p + J_{leak} + \sum_{i,j}\sigma(x_i, y_j)S(x_i, y_j, t; T_{open})\delta(x - x_i)\delta(y - y_j). \quad (1)$$

The summation term is new to this paper. Each term in the summation represents a point source (the CRU) located at the lattice site (x_i, y_j) that produces a molar flux σ. The lattice sites are spaced ℓ_x apart (2 μm, the sarcomere length) along the longitudinal axis of the cell (*x*-axis) and ℓ_y apart (0.4 or 0.8 μm) in the transverse direction (*y*-axis). Figure 3, *inset,* and Fig. 4 show the lattice. CRUs on a column (fixed *x*) are said to be on a *z*-line. *S* is a stochastic function taking values of either 0 or 1, so switches the CRU on (firing) or off. After *S* becomes 1, it stays at this value for time T_{open}. The probability that the CRU will fire in time Δt is $P(C(x, y, t), K, n) \cdot \Delta t$, where *P* is the probability of firing per unit time. *P* is a function of the ambient Ca^{2+} concentration $C(x_i, y_j, t)$ and is given by

$$P(C(x, y, t), K, n) = \frac{P_{max}C^n}{K^n + C^n}. \quad (2)$$

P was determined as follows. Let *r* be the number of sparks/100 μm linescan/ms. Assume that the microscope's lateral (*y*) and axial resolution (*z*) is 0.5 and 1 μm, respectively. If CRUs are arranged in a square lattice on the *z*-line plane with spacing ℓ_y = 0.8 μm, then there will be $\sim$2 CRUs (or $\sim$6 for ℓ_y = 0.4) in a 0.5 μm × 1 μm confocal sample area at each *z*-line. Assuming a sarcomere length of ℓ_x = 2 μm, then, in a 100-μm

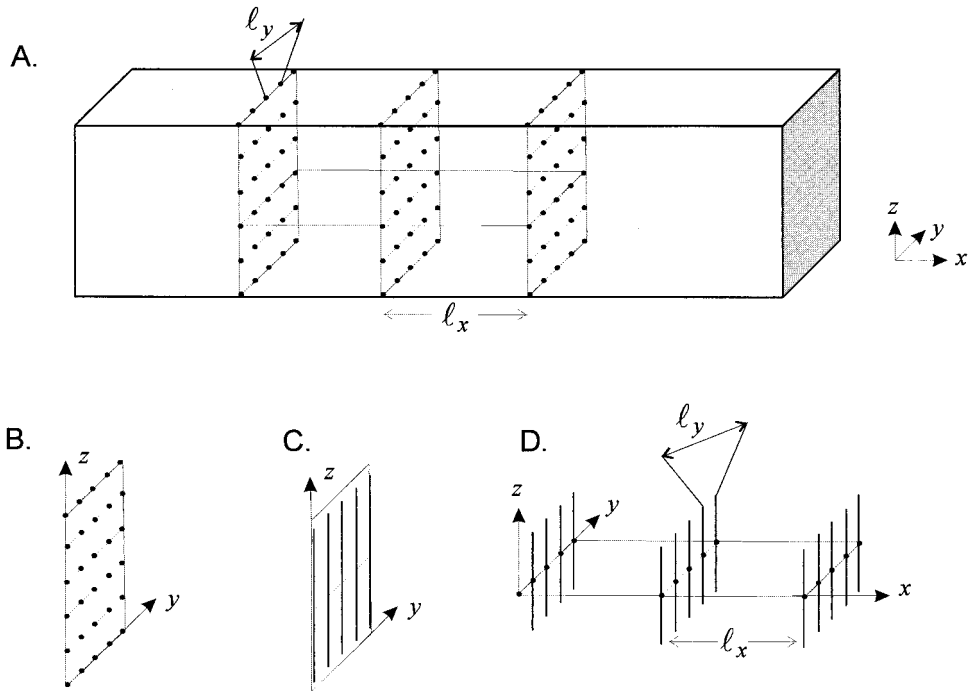

FIGURE 1 Geometry of model.(*A*) Three-dimensional schematic of a cardiac ventricular cell. The longitudinal axis of the cell is in the *x*-direction. The three vertical planes represent the *z*-lines and are spaced a distance of ℓ_x (= 2 μm) apart. The *y*–*z* plane at the *z*-line contain the CRUs (*dots*) that are symmetrically spaced along the *y* and *z* directions. The horizontal plane shown in the center is the domain on which the model equations are defined. (*B*) An individual *y*–*z* plane and its CRUs. Ca^{2+} release by discrete CRUs will generate concentration gradients in all directions. To eliminate gradients along *z*, the discrete CRUs along *z* are replaced by line sources that extend from $-\infty < z < \infty$ as shown in *C*. (*D*) The 2D slice of the ventricular cell with CRUs represented by line sources spaced ℓ_x apart along *x* and ℓ_y (= 0.4 or 0.8 μm) along *y*.

confocal linescan, there are N_{CRU} = 2 CRU/*z*-line × 50 *z*-lines/100 μm linescan = 100 CRU/100 μm linescan. Then $P = r/N_{CRU}$. Note that P_{max} has units of sparks/ms/CRU. The spark rate, the Hill coefficient n = 1.6 and the Ca^{2+}-sensitivity factor K = 15 μM are taken from Lukyanenko and Györke (1999). Using a spark frequency of 10 sparks/100 μm linescan/s at a Ca^{2+} concentration of 100 nM, for N_{CRU} = 1 CRU/μm, P_{max} equals 0.3/CRU/ms (or 0.05/CRU/ms for ℓ_y = 0.4). Note that P_{max} is kept at these values (0.3 or 0.05) in simulations where K is varied.

The source strength σ requires some explanation. Because a line source is not equivalent to a linear array of discrete CRUs (shown in Fig. 1 *B*), we need to somehow adjust the molar flux of the line source to approximate the molar flux of a point source. If Ca^{2+} were being released from a CRU into a 3D volume, then $\sigma_3 = I_{SR}/2F$, where I_{SR} is the current and F is the Faraday. Note that σ_3 has units of mole/ms. Because the model is 2D, $\sigma = \sigma_2$ has units of mole/ms/μm. What value should we use for σ_2 in place of σ_3? Although no value of σ_2 will give the identical space–time Ca^{2+} distribution in 2D as σ_3 will in 3D, we define an "equivalent" source strength σ_2 as one that gives the same concentration as σ_3 at $r = \bar{r}$ (the Euclidean distance) and $t = \bar{t}$ in a linear system. Let $C(r, t, d)$ be the concentration at (r, t) in d = 2, 3 dimensions. Then $C(r, t, 3) = (\sigma_3/(4\pi Dr))\text{erfc}(z)$, $C(r, t, 2) = (\sigma_2/(4\pi D))E_1(z^2)$ where $z = r/\sqrt{4Dt}$ and E_1 is the exponential integral (Appendix A). For $\bar{r}$ = 0.5 μm, $\bar{t}$ = 5 ms, and D = 0.2 μm^2/ms (the geometric mean of D_{Cx} and D_{Cy}), σ_2 = 0.64 σ_3/μm. We used this numerical conversion in all our simulations. With this conversion factor, the sparks in the 2D model has about the same spatial spread and time course as the 3D spark. For example, for I_{SR} = 20 pA the spark FWHM along *x* at the end of 5 ms was 2 μm in 3D (Izu et al., 2001) and 1.9 μm in 2D.

We will vary I_{SR}, T_{open}, K, and ℓ_y. The remaining parameters use the following (standard) values (see Izu et al., 2001 for references): ℓ_x = 2 μm (Shacklock et al., 1995), n = 1.6 (Lukyanenko and Györke, 1999), H_B = 123 μM, k_B^+ = 100/μM/ms, k_B^- = 100/ms, H_D = 50 μM, k_D^+ = 80 μM/s, k_D^- = 90/s, V_p = 200 μM/s, K_p = 184 nM, n_p = 4, D_{Cx} = 0.3 μm^2/ms, D_{Cy} = 0.15 μm^2/ms, D_{Dx} = 0.02 μm^2/ms, and D_{Dy} = 0.01 μm^2/ms, and C_0 = 0.1 μM.

We used the reaction of Ca^{2+} with fluo-3 described by Smith et al. (1998) instead of the more complex set of reactions proposed by Harkins et al. (1993) because of computational limitations. In our companion paper (Izu et al., 2001), we found that the Harkins buffer model produced sparks with more realistic *F*/*Fo* and slightly larger spatial spread than did the Smith model. However, computations took considerably longer with the Harkins model and required a finer spatial discretization than the Smith model, making the computational costs prohibitive. We consider possible ramifications of using the Harkins model in the Discussion.

Numerical methods

The model equations were discretized and numerically solved using Facsimile as described in Izu et al. (2001). The stochastic opening of a CRU was simulated as follows. At regular intervals of time Δt (typically 1 ms), a uniformly distributed random number u between 0 and 1 is generated. Note that, as $C \to \infty$, $P/P_{max} \to 1$ so the probability that u is less than P/P_{max} approaches 1. Thus, the CRU fires when $u < P/P_{max}$ by setting S to 1, and S remains unity for T_{open} ms. After closing, the channel does not reopen.

The computational grid was a rectangle 20 μm × 20 μm with mesh size of 0.1 μm along both *x* and *y* directions. We were constrained to use these small domains because a typical simulation of 150 ms takes ~24 hrs on a 400 MHz Pentium II processor with 256 MB RAM, and computation time

grows faster than computational area. Neumann boundary conditions were imposed on all edges.

RESULTS

The basic principle behind wave evolution in this model is simple. Waves originate and are sustained as Ca^{2+} released from one or more CRUs diffuse to neighboring CRUs and raise the probability that these neighbors will release Ca^{2+} (or "fire") and, in turn, induce other neighbors to fire. Our model of Ca^{2+} waves is analogous to piles of gunpowder wherein igniting one pile may ignite the neighboring pile. The probability that the neighbor will ignite depends on how far the piles are from each other (ℓ_x, ℓ_y), the rate of heat production (I_{SR}), the total amount of heat produced from each pile ($I_{SR} \times T_{open}$), and the thermal stability of the gunpowder (K). The challenge is to get a quantitative understanding of the conditions needed to initiate a wave, of how the wave evolves, the wave velocity, etc.

We start by analyzing a deterministic linear model for waves on lattices even though it turns out to be inadequate for understanding waves in muscle cells for the following reasons.

1. The linear analysis is a natural first attempt because linear systems are simple and exactly solvable. So if they prove to be accurate descriptions of waves in nonlinear systems, then virtually everything about waves will be known.
2. Because the linear solution is given in terms of known functions (see Eq. 3), it provides a standard to check the accuracy of the numerical algorithm used to solve the model equations.
3. Most importantly, the failure of the linear approximation to accurately predict properties of waves in the nonlinear system reveals an essential difference between nonlinear and linear systems: superadditivity. We examine the origin of superadditivity and show its importance in understanding waves in cells.

Next, we examine the propagation of a Ca^{2+} wave and extract the basic steps in the propagation of waves on rectangular lattices. Because the firing of CRUs is stochastic, we need to develop the probabilistic machinery to estimate whether a given set of model parameters will be able to support a wave, predict the wave's speed, and estimate the number of CRUs required to trigger a wave.

Linear systems

We would know virtually everything about waves if we could predict the Ca^{2+} concentration at any point (x, y, t) given the history of firings of CRUs. This prediction is not possible in nonlinear systems but is possible in linear systems. Linear systems, endowed with the property of additivity, allow us to calculate $C(x, y, t)$ knowing the space–time distribution of Ca^{2+} from a single spark. $C(x, y, t)$ is given by

$$C(x, y, t) = \sum_{i,j} \frac{q_{ij}}{4\pi\sqrt{D_x D_y}} \tilde{E}_1(x_i - x, y_j - y, t - t_{ij}, T_{open}) + C_0. \quad (3)$$

The addend, derived in Appendix A, gives the space–time Ca^{2+} distribution for a single CRU with constant molar flux q_{ij} that is open for time T_{open}. Note that the solution takes account of anisotropic diffusion. The summation is taken over all sites that have fired. t_{ij} is the time the channel at (x_i, y_j) had fired. This fundamental equation contains all the information about wave propagation on discrete lattices in a linear deterministic system.

The analytic power of linear systems stems from the ability to predict the Ca^{2+} concentration at any point (x, y, t) due to the firing of an arbitrary distribution of CRUs given the Ca^{2+} distribution due to a single CRU. The objective here is to fit the Ca^{2+} distribution from a single spark in the presence of buffers and pump (nonlinear system) to that of a linear system (see Appendix A),

$$C(x, y, t) = \frac{q}{4\pi\sqrt{D_x D_y}} \tilde{E}_1(x, y, t, T_{open}), \quad (4)$$

that defines an equivalent flux q and diffusion coefficient D_x. D_y always equaled $D_x/2$. Figure 2, *A* and *B,* show the concentration profiles from the simulations (*circles*) and the fitted function (*solid curve*) at $t = 5$ ms (*left profile*) and 10 ms (*right profile*) after the channel opens. Panel *A* shows the profile along x, and *B*, the profile along y. Figure 2, *C* and *D,* show q and D_x; in a linear system, these parameters would be time independent. Note that the values of D_x and q determined from the x profile (*up triangle*) and y profile (*down triangle*) are almost identical. This equality is important because it means that the Ca^{2+} concentration at an arbitrary point (x, y, t) can be calculated using Eq. 3 using a single pair (q, D_x) for any given moment. Time-dependent changes in q and D_x simply arise from fitting the solution to the nonlinear problem to that of a linear problem. If the buffers were absent, then the system would be linear and q and D_x would be invariant. There is no simple physiological interpretation for the time dependency of q and D_x.

It is important to observe in Fig. 2 that the Ca^{2+} concentration is a very steep function of distance; it drops 1000-fold within 1.5 μm from the source. A CRU at $x = 2$ μm would "see" a Ca^{2+} concentration of just 179 nM, 10 ms after the channel opens. Even if this concentration could be maintained indefinitely, the mean waiting time for the CRU to fire is $1/P(179\ \text{nM}, 15\ \mu\text{M}, 1.6) = 3.98$ s (see Appendix B), so a single spark is unlikely to trigger a spark at an adjacent sarcomere. This calculation is in accord with Parker et al.'s (1996) observation that the probability of a spark triggering another 2 μm away was zero.

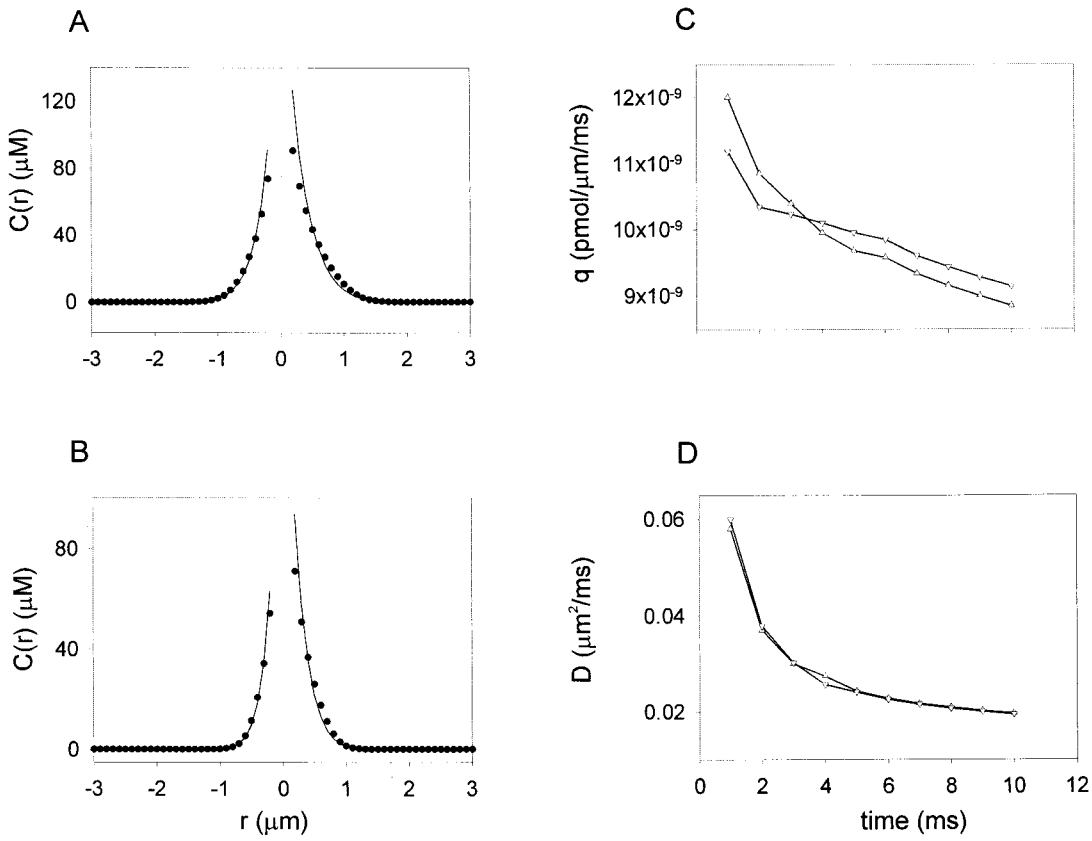

FIGURE 2 Determination of "equivalent" q and D_x. Single spark profiles from simulations (*circles*) were fit to Eq. 4 by adjusting q and D_x. (*A*) The profile along x at $t = 5$ ms ($r < 0$) and $t = 10$ ms ($r > 0$). (*B*) Similar to *A*, but shows the profile along y. The best fit values of q and D_x as functions of t are shown in *C* and *D*. Up-triangles show the fit of the spark profile along x; down-triangles, along y. Simulations carried out using $I_{SR} = 20$ pA, $T_{open} = 10$ ms.

Triggering of sparks on adjacent sarcomeres is the *sine quo non* of wave propagation in our model. Thus multiple channels must fire within a short time interval to raise the Ca^{2+} concentration at an adjacent sarcomere enough to trigger Ca^{2+} release. We calculated $C(x, y, t)$ using Eq. 3 and q, D_x values at $t = 10$ ms for different configurations of simultaneously firing CRUs shown in Fig. 3. The channel configurations are labeled (*a*) 1×1, (*b*) 1×3, (*c*) 1×7, (*d*) 2×7, and (*e*) 1×9, where the first and second numbers refer to the number of columns and rows of CRUs, respectively. The inset in Fig. 3 shows a schematic of the lattice, the arrangement of CRUs in a 2×3 configuration. The CRUs in a column are symmetrically displaced about the origin so, for example, the coordinates of the 3 CRUs in the 1×3 configuration are $(0, 0)$, $(0, +\ell_y)$, and $(0, -l_y)$, where $\ell_y = 0.8$ μm. The rationale for choosing these configurations will become evident later. For configuration (*d*) the 2 columns are at $x = 0$ and -2 μm. Fig. 3 *A* shows the concentration along the x-axis ($y = 0$) at $t = 10$ ms for configurations (*a–e*). Because of the steep Ca^{2+} concentration profile, the firing of additional CRUs in *b–e* do not add substantially to the concentration due to the single CRU at the origin (*a*, *lower curve*). At this resolution, the profiles for channel configurations b, c, d, and e are indistinguishable. Thus the linear model predicts that none of these configurations of firing channels could raise the Ca^{2+} concentration at $x = 2$ μm sufficiently to substantially increase the probability of firing within 10 ms.

Superadditivity in buffered systems

A buffered system behaves differently, however. Fig. 3 *B* shows Ca^{2+} concentration profiles derived from simulations of the nonlinear system (buffers reactions and pump included) for the same five configurations (the graphs for *c* and *e* are virtually identical). In contrast to the linear system, the firing of the flanking CRUs greatly increased the Ca^{2+} concentration along the x-axis.

The concentration profiles in Fig. 3 *A* are expected if the effect of two or more sparks were additive. However, Fig. 3 *B* shows that the actual concentration exceeds the expected values. We call this property *superadditivity*. Superadditivity arises simply because the free Ca^{2+} buffers

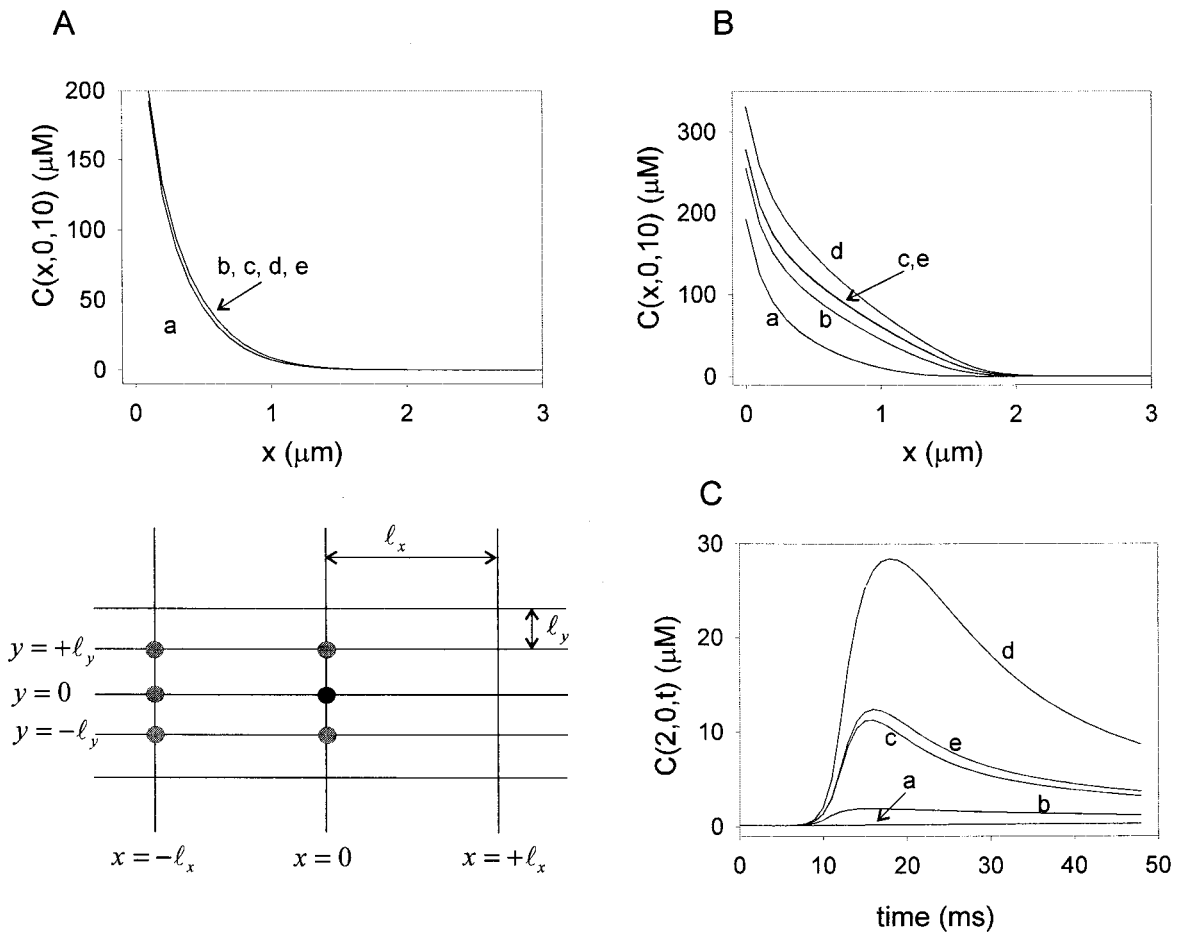

FIGURE 3 Ca^{2+} concentration ($C(x, y, t)$) in (*A*) additive and (*B, C*) superadditive systems. (*A*) and (*B*) show the Ca^{2+} spatial distribution along x at $y = 0$ at $t = 10$ ms due to firing of CRUs in the following configurations: (a) 1×1, (b) 1×3, (c) 1×7, (d) 2×7, and (e) 1×9. Inset, a schematic of the lattice with a 2×3 configuration of CRUs. The darker circle indicates the CRU at the origin. In an additive system (*A*) simultaneous firing of multiple CRUs (b–e) do not add significantly to the Ca^{2+} concentration from a single CRU (a). A buffered system exhibits superadditivity, and the Ca^{2+} distribution due to firing of multiple CRUs is remarkably different. Note that there is little difference due to firing of 7 or 9 CRUs (c, e). (*C*) The temporal behavior of the Ca^{2+} concentration at $x = 2$, $y = 0$ in a buffered system. Simulation parameters: $I_{SR} = 20$ pA, $T_{open} = 10$ ms.

become depleted. The addition of m moles of Ca^{2+} causes a drop in the available free buffer, so subsequent additions of m moles result in a larger increase in the Ca^{2+} concentration.

A consequence of superadditivity important for understanding Ca^{2+} wave propagation is that, when CRUs fire simultaneously, the range of Ca^{2+} signaling increases tremendously. This is seen in Fig. 3 *B* and is also illustrated in Fig. 3 *C,* where the concentration at ($x = 2$ μm, $y = 0$) is plotted against time. Note the tremendous amplification in the Ca^{2+} concentration as more CRUs fire. The maximum concentration attained 2 μm away from a single spark is 278 nM (*a*), whereas, at the same distance from the center of seven sparks (*c*), the maximum concentration is 11.3 μM, 41 times larger.

Wave propagation in nonlinear systems

For a linear (additive) system, we can make a priori predictions of wave properties, such as the wave speed based on the properties of a single spark. However, because of superadditivity in buffered systems, such predictions are not possible. This does not mean, however, that there are no predictive tools for nonlinear waves. Instead, the probabilistic tools we will develop below require more information than that provided from a single spark as input data and require some knowledge of how waves propagate on lattices. Thus we first examine in detail how a wave propagates on a rectangular lattice. Once we understand the basic steps of wave propagation, we can set up approximations to the Ca^{2+} distribution in a wave, which are used in the probabilistic equations. These equations are used to predict wave properties, such as whether waves can exist for a given set of parameters and the wave velocity.

Before proceeding, let us explain why we need these predictive tools and why we cannot rely solely on numerical solutions of the nonlinear model equations. The primary reason is that these tools give us insight into the factors that

shape the evolution of waves. The second reason is pragmatic. A typical simulation takes about 24 hrs of computation time, so we rely on our predictive tools to guide us in making judicious parameter choices. The input data for the probabilistic equations require only about 1 hr to compute.

Basic steps in propagating waves on discrete rectangular lattices

Figure 4 shows how a Ca^{2+} wave propagates on a discrete rectangular lattice. The 11 images are of the Ca^{2+} concentration distribution in the x–y plane at $t = 0$, 26, 29, 34, 38, 55, 65, 75, 85, 95, and 105 ms (*left* to *right, top* to *bottom*). The white dots are the locations of the CRUs spaced 2 μm apart longitudinally and 0.8 μm apart transversely. The white curves show where C is between 10 μM and 20 μM. The origin is at the lower left corner. At $t = 0$, $C(x, y, 0) = 0.1$ μM except on the 4×4 μm^2 square at the origin where $C = 30$ μM. Note that the buffers are in equilibrium with the Ca^{2+} everywhere. We pick up the progress of the wave at $t = 26$ ms where we see five firing CRUs at $x = 6$ μm; the CRU at $y = 2.4$ μm fired at $t = 15$ ms and is no longer releasing Ca^{2+}. At this time there is a "wall" of high Ca^{2+} concentration (*white curve*) bearing down on the CRUs at $x = 8$ μm. The next three images at $t = 29$, 34, and 38 ms illustrate the rapid activation of six contiguous CRUs along $x = 8$ μm. This rapid activation is shown also in the 12th image, which is a transverse linescan through $x = 8$ μm. This linescan image is oriented with the y-coordinate in the same direction as the x–y images, so there is a point-to-point correspondence with the x–y image. The six contiguous CRUs fire in rapid succession, giving rise to the nearly flat apex of the transverse wave.

In the 5th image ($t = 38$ ms), there is the wall of high Ca^{2+} concentration approaching the CRUs at $x = 10$ μm. In time, CRUs at $x = 10$ μm will fire, sending out another wall of Ca^{2+} to $x = 12$ μm, thus regenerating the cycle of wave propagation.

The sequence of events just described—firing of 5–7 contiguous CRUs in rapid succession, generating a wall of high Ca^{2+} that, in turn, triggers CRU firing at the next sarcomere—is the basic pattern for Ca^{2+} wave propagation

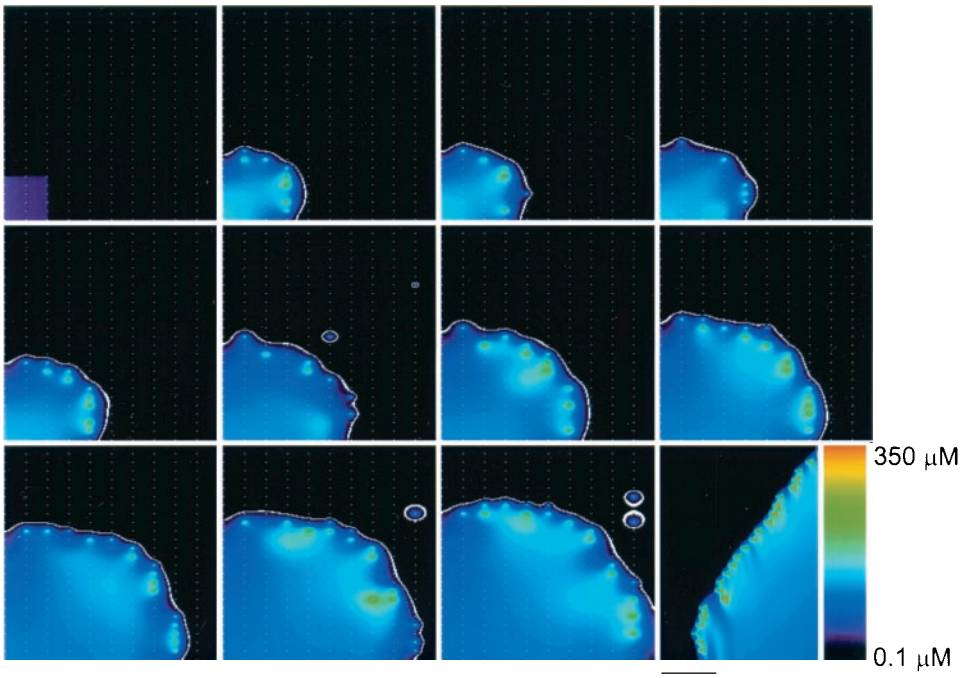

FIGURE 4 Wave propagation on rectangular lattices. These snapshots of Ca^{2+} distribution in the x–y plane were taken at 0, 26, 29, 34, 38, 55, 65, 75, 85, 95, and 105 ms (*left* to *right, top* to *bottom*). The white dots are the locations of the CRUs spaced 2 μm apart longitudinally and 0.8 μm apart transversely. The white curves show where $10\ \mu M < C < 20\ \mu M$. The simulation starts with C set to 30 μM on $0 < x < 4$ μm, $0 < y < 4$ μm (image 1); buffers (endogenous and fluo-3) are in equilibrium with Ca^{2+}. Elsewhere, all chemical species are set to their baseline values. Images 2–5 illustrate how Ca^{2+} waves propagate on rectangular lattices. Image 2 shows a "wall" of high Ca^{2+} concentration (*white curve*) bearing down on the column of CRUs at $x = 8$ μm. This wall of Ca^{2+} causes the nearly simultaneous activation of about 7 CRUs (images 3–5). The sequence of firings along $x = 8$ is shown in the transverse linescan (image 12, time flows from *left* to *right*). The near simultaneous firing of ~6 CRUs shows up as the flat part of the linescan image. Subsequently, CRUs along y fire sequentially at nearly regular intervals, seen as the sloping part of the linescan image. About 5–7 contiguous CRUs are needed to raise the Ca^{2+} concentration high enough to trigger CRUs 2 μm away at the next column to sustain the wave as was seen in the previous figure. Note spontaneous sparks occur in images 6, 10, and 11. "Jumping" of the wave from one column to the next is not evident in these static images; this solution and others in the form of MPEG movies can be downloaded from our ftp site ftp://ntcv.umaryland.edu/pub/izu/. (The readme.txt file gives a guide to the movies.) The scale bar in panel 12 represents 50 ms.

on lattices. To generate enough Ca^{2+} to saturate the buffers and to sufficiently raise the Ca^{2+} concentration at the next sarcomere, about 5–7 CRUs must fire in rapid succession as was seen in Fig. 3 *C*, illustrating superadditivity.

The rapid firing of 5–7 contiguous CRUs on a *z*-line shows up as the flat apex in a transverse linescan image (image 12, *left-hand side*). However, after this initial flurry of firings, subsequent firings on that *z*-line occur in a step-by-step fashion at regular intervals as shown in the sloping edge of the linescan image.

Images 6–11 are taken at 10-ms intervals and illustrate the steady progression of the wave. Two spontaneous sparks are seen in image 6 ($t = 55$ ms) at (10, 9.6) (near the center) and at (18, 14.4). The elliptical diffusion of Ca^{2+} is clearly seen in the (10, 9.6) spark. These sparks do not trigger firing from adjacent sarcomeres 2 μm away. In the 10th ($t = 95$ ms) image image a spark occurs at (18, 13.6) and, in the 11th ($t = 105$ ms) image, sparks occur at (18, 15.2) and (18, 12.8). The sparks at (18, 13.6), (18, 15.2), and (18, 12.8) were probably triggered by the spark at (18, 14.4). Using the probabilistic equations in the next section, we calculate the probability of these CRUs firing to be ~0.5. In contrast, the probability of firing of a CRU far from the (18, 13.6) spark, say at (12, 14.4), during $55 < t < 105$ is only 0.014. Animated images of the simulation shown in Fig. 4 and other simulations, in the form of MPEG movies, can be downloaded from our ftp site ftp://ntcv.u-maryland.edu/pub/izu/.

Wave statistics

Earlier deterministic models for Ca^{2+} wave propagation (Backx et al., 1989; Keizer et al., 1998; Lukyanenko et al., 1999) assumed that the CRU fires as soon as the local Ca^{2+} concentration exceeds the threshold C^*. In a stochastic system, this would be true if n were so large that $P(C, K, n)$ would be nearly a step function with $C^* \approx K$. Because $n \sim 2$, however, $P(C, K, n)$ has a shallow slope, so there is a distribution of times before a CRU fires. Thus exactly when a CRU will fire cannot be known, so, instead, we calculate the probability of firing within some time interval.

If the Ca^{2+} concentration at a CRU is fixed at $\bar{C}$, then the waiting time before it fires follows an exponential distribution and the mean waiting time (MWT) before firing is $1/P(\bar{C}, K, n)$. This standard result is not applicable to studying waves because the Ca^{2+} concentration at a CRU varies with time. In Appendix B, we derive, assuming time-varying $P(C, K, n)$, expressions for $p(x, y, t < \tau)$, the probability that a CRU at (x, y) does not fire in time $t < \tau$ (Eq. B3); $\varphi(x, y, t)$, the waiting time distribution (Eqs. B5 and B8); the MWT before the CRU fires (Eq. B6), and $P(X \geq 1, t < \tau)$, the probability that at least one CRU has fired in time $t < \tau$ (Eq. B7).

Effect of I_{SR} and T_{open} on waves

We apply these formulas to study the effects I_{SR} and T_{open} have on waves. First, we approximate the Ca^{2+} distribution in a wave whose front is at column $i = 0$ by two methods. In method *a* we simultaneously fire two columns of seven contiguous CRUs ($y = \ell_y j$, $j = -3, \ldots, 3$, $x = -\ell_x$ and $x = 0$); in method *b* we fire one column of seven CRUs ($y = \ell_y j$, $j = -3, \ldots, x = 0$) and set the initial Ca^{2+} (and the other chemical species) to a high value, comparable to that seen in waves, in the region $x < 0$, $-3\ell_y < y < 3\ell_y$. The choice of seven CRUs comes from observing, in Ca^{2+} waves, that ~5–7 CRUs must fire on column i before any CRU on column $i + 1$ fires. In method *b*, the choice of the initial Ca^{2+} concentration is arbitrary, but the range is guided by results from some simulations. The distribution in *a* was chosen to approximate the distribution in a nascent wave, whereas that in *b*, a well-developed wave. Needless to say, both methods approximate the concentrations in a wave very crudely, but they nevertheless provide useful guides in choosing model parameters for simulations. The time cost of these rough calculations, ~1–2 hrs, is well warranted before carrying out an ~24–36-hr simulation.

Method *a* underestimates the velocity because the Ca^{2+} concentration gradient on $x < 0$ is greater than that in a wave, so less Ca^{2+} flows to the CRUs on column $i + 1$. Method *b* overestimates the velocity because, in a wave, the CRUs on the wave front fire in rapid succession but not simultaneously as assumed in method *b*. Thus, the velocity from the simulation is bracketed by the estimates from the two methods.

Each CRU at ($x = 2$, $y = 0.8j$), $j = -3, -2, \ldots, 2, 3$ sees a changing Ca^{2+} concentration similar to that in curve *d* in Fig. 3 *C*. Knowing $C(x = 2, y = 0.8j, t)$, we then calculate the probability that at least one CRU at $x = 2$ will fire within τ ms, $P(X \geq 1, t > \tau)$. The waiting time distribution (WTD) φ before a CRU at $x = 2$ fires is then used to calculate the MWT for firing.

Figure 5 *A* shows the probability of at least one firing and 5 *B* the waiting time distributions for different combinations of (I_{SR}, T_{open}). The curves labeled with circles, squares, and down-triangles derive from $I_{SR} = 20$ pA and $T_{open} = 8$, 7, and 5 ms, respectively. The curve with up-triangles comes from (15, 8). The *a* and *b* sublabels signify the method used to generate the concentration distributions. These curves illustrate the striking sensitivity of $P(X \geq 1, t < \tau)$ and the WTDs to I_{SR} and T_{open}.

First consider the case where $I_{SR} = 20$ pA and $T_{open} = 8$ ms (*circles*). Using the distribution of method *a*, we see (*Aa*) the probability of firing starts rising starting ~10 ms after the channels at $x = 0$ and $x = -2$ have fired, and, by 20 ms, it is almost certain that at least one CRU at $x = 2$ has fired. The WTD φ (*Ba*) also rises rapidly, peaks at 15 ms, then declines rapidly. The decline of φ to almost zero beyond ~25 ms means that the probability of needing to wait more than 25 ms before a CRU fires is virtually zero. The MWT

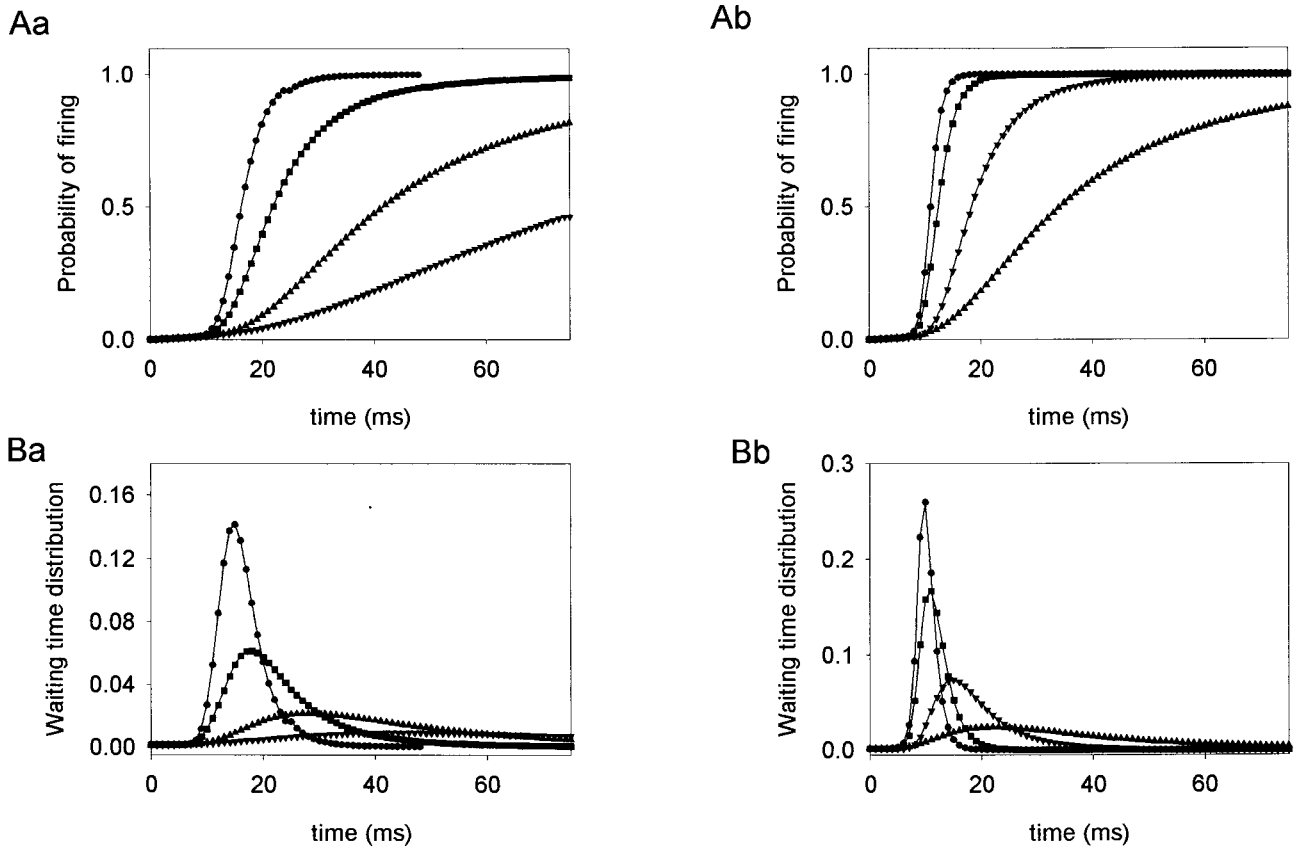

FIGURE 5 Probability of firing (*Aa*, *Ab*) and waiting time distributions (*Ba*, *Bb*) for different combinations of (I_{SR}, T_{open}). The sublabels (a,b) refer to the method the Ca^{2+} concentration in the wave was approximated (see text). *Circles,* (I_{SR}, T_{open}) = (20, 8); *squares,* (20, 7); *up-triangle,* (15, 8); *down-triangle,* (20, 5).

for this distribution is 15.89 ± 4.47 ms, from which we estimate the longitudinal velocity by $\nu_x = \ell_x/\text{MWT} = 2$ μm/15.89 ms = 126 μm/s.

The parallel calculations of $P(X \geq 1, t < \tau)$ and φ using the distribution of method *b* are given in *Ab* and *Bb*. The CRUs at $x = 2$ see a higher Ca^{2+} concentration than in method *a* because the shallower concentration gradient on $x < 0$ causes the large amount of Ca^{2+} in the reservoir ($x < 0$, $-3\ell_y < y < 3\ell_y$) and Ca^{2+} released from the CRUs to flow mostly rightward. Not surprisingly then, $P(X \geq 1, t < \tau)$ approaches 1 more quickly, and φ is sharper for method *b*. The MWT is now 10.06 ± 1.91 ms and the estimated velocity is 199 μm/s. The wave velocity measured in a simulated wave (see below) with these parameters was 155 μm/s, which is between the estimates from methods *a* and *b*.

Firing properties change dramatically when T_{open} decreases by just 3 ms from 8 ms to 5 ms (*down triangles*). Whereas the probability of CRU firing at $x = 2$ was almost 1 at $t = 20$ ms for $T_{open} = 8$ ms, when $T_{open} = 5$ ms, the probability of firing does not reach 0.5 until 80 ms using method *a* or 37 ms using method *b*. Note the waiting time distributions are very broad with a barely perceptible peak at 22 ms (*Bb*) and 47 ms (*Ab*). The MWTs are 69.03 ± 35.40 ms (*a*) and 40.63 ± 30.22 ms (*b*). The broad waiting time distributions mean that a CRU at $x = 2$ will have an equally low chance of firing at almost any time after ~10 ms after CRUs at $x = -2$ and $x = 0$ have fired.

We do not expect waves to propagate with perfect regularity in a stochastic system, but there must be a modicum of predictability. The broadening of the waiting time distribution curves signals loss of predictability. For the parameter pairs (20, 5) and (15, 8), *down-* and *up-triangles,* the waiting time distributions are so broad that they preclude a reasonable estimate of the time a wave front will reach the next column of CRUs. Hence these calculations indicate that Ca^{2+} waves are unlikely to occur with these parameter combinations. These predictions were confirmed by simulations started with method *a*.

Physiological meaning of the waiting time distributions

We get a clearer understanding of the physiological meaning of the WTDs by examining them in conjunction with

linescan images of Ca^{2+} waves shown in Fig. 6. The three waves were produced with parameter combinations (I_{SR} = 20 pA, T_{open} = 8 ms) (panel *Aa*), (20, 5) [panel *Ba*], and (5, 32) (panel *Ca*). These linescans are oriented with time flowing from left to right, and the linescan was along the longitudinal axis at y = 2.4 μm. In Panel *A* the wave produces a sharp edge in the linescan image whose slope (measured with respect to the horizontal) equals the wave velocity of 155 μm/s. The sharpness of the edge stems from the almost perfectly regular firing intervals between CRUs shown in the accompanying time plot of the Ca^{2+} concentration at the release sites at x = 6, 8, 10, . . . , 18 μm (Fig.

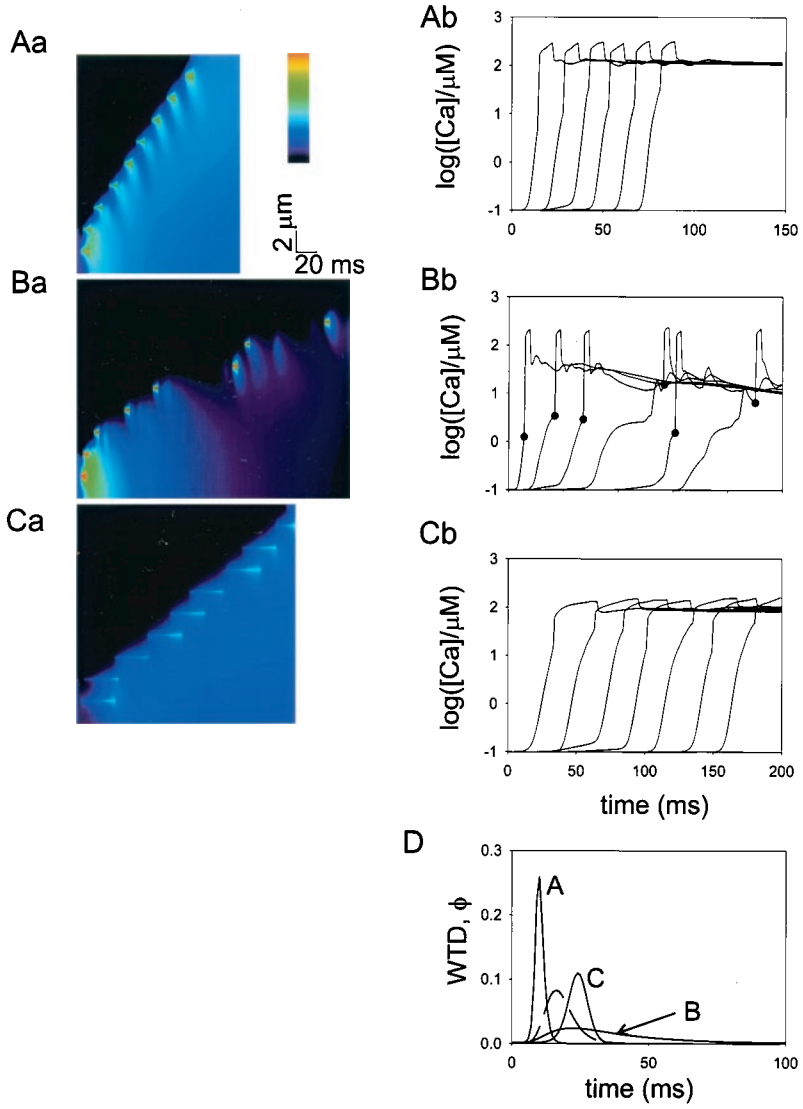

FIGURE 6 Regularity of wave propagation for different (I_{SR}, T_{open}). Local variations in the wave velocity are reflected in the longitudinal linescan images *Aa* (I_{SR} = 20, T_{open} = 8), *Ba* (20, 5), and *Ca* (5, 32). In *Aa*, the wave front progresses from *z*-line to *z*-line (bright spots showing CRU firing) at a regular pace, giving rise to a sharp edge in the linescan image. *Ab* is the corresponding time plot of log($C(x, y = 2.4, t)$) for x = 6, 8, 10, . . . , 16 μm showing the wave moving with almost deterministic precision despite the firing of CRUs being a random variable. The mean time between firings is 14.1 ms with standard deviation (SD) of only 2.1 ms. This great regularity is predicted from the very narrow waiting time distribution (WTD), curve A, *panel D*, calculated using an approximation of the Ca^{2+} distribution in a wave using method *b* (see text for explanation). *Ba* shows a ragged wave indicating very irregular wave propagation caused by reducing T_{open} by just 3 ms to 5 ms. The time plot of log($C(x, y = 2.4, t)$) (*Bb*) shows not only large variability in the time of CRU firing but also the local Ca^{2+} concentration at the time of firing (*circles*). Note that the CRU at x = 12 sees a Ca^{2+} of 3 μM for ~30 ms but does not fire until $C \approx 10$ μM. The mean time between firings is 41.6 ms with a large SD of 29.1 ms. The WTD (curve B, *panel D*) is also very broad; its mean is 40.6 ms and SD is 30.2 ms. The parameters for wave C were chosen so that the total Ca^{2+} released, $I_{SR} \times T_{open}$, was the same as in A. Although the parameters for A and C appear vastly different, the waves are more similar to each other than the wave in B. Linescans A and C are scaled between 0.1 and 350 μM and are about equally bright because the total Ca^{2+} released is identical; linescan B is scaled between 0.1 and 175 μM and is considerably dimmer than A and C. C's wave velocity (81 μm/s) is about half of A's (155 μm/s) reflecting the slower rate of release (I_{SR}), but the wave front is quite sharp. The mean time between firing (from the time plot *Cb*) is 24.6 ms with SD = 8.4 ms; the WTD has mean of 23.3 ms and SD of 4.6 ms.

6 *Ab)*. The mean time between firings is 14.1 ms with a standard deviation (SD) of 2.1 ms. In this and remaining time plots, the Ca^{2+} concentration rises rapidly in the first few milliseconds after the CRU fires, then more slowly as diffusion balances influx. The sudden drop occurs when the CRU closes.

In contrast to this wave that propagates with almost deterministic precision, the wave in Fig. 6 *Ba* propagates unpredictably. The unpredictable timing of firing of successive CRUs is seen in the time plot (Fig. 6 *Bb*) and gives the linescan image a ragged edge. The stochastic nature of CRU firing is clearly evident in the time plot. Note that the Ca^{2+} concentration at which the CRU fires (*circles*) varies widely from 1.3 to 15.3 μM. The CRU at $x = 12$ μm (4th curve from left) sees a Ca^{2+} concentration of $\sim$2 μM for $\sim$30 ms without firing, although CRUs at $x = 6$, 8, and 10 μm had fired at this concentration. In fact, the CRUs at $x = 12$ and 16 μm do not fire until the Ca^{2+} concentration is raised by the firing of neighboring CRUs (off of the linescan) to $\sim$10 μM.

The widely differing firing patterns of waves in *Aa* and *Ba* are reflected in their respective WTDs shown in Fig. 5 and reproduced in Fig. 6 *D*. The nearly fixed firing intervals in *A* can be anticipated from the narrow WTD, which has a SD of 1.91 ms, close to the measured dispersion of firing intervals in the wave. The mean of this WTD (i.e., the MWT) is 10.9 ms, somewhat less than the mean firing interval. As mentioned earlier, the MWT calculated using method *b* overestimates the wave speed.

The WTD for (20, 5) (*curve B*) is very broad; its mean is 40.6 ms with a SD of 30.2 ms. The large dispersion in the WTD is the reason for the large variability in firing intervals for the wave in Panel *B*. The MWT and SD for WTD (*B*) are close to the mean firing interval measured from time plot *Bb* of 41.6 ms with SD of 29.1 ms.

Total Ca^{2+} released is a strong determinant of wave properties

The waves in panels *A*, *B*, and *C* of Fig. 6 were generated with (I_{SR}, T_{open}) of (20, 8), (20, 5), and (5, 32), respectively. Although the parameters are similar for *A* and *B*, the waves are quite different. In contrast, (20, 8) and (5, 32) are dissimilar yet the waves they engender are similar in terms of their regularity. What is common to both (20, 8) and (5, 32) parameter sets is the total amount of Ca^{2+} released per CRU ($I_{SR} \times T_{open}$) is the same. The mean and SD for the (5, 32)-WTD, curve *C*, are 23.33 and 4.55; the mean firing interval measured from the time plots in Fig. 6 *Cb* is 24.56 ms and the SD is 8.44 ms. We expect that the MWT for (5, 32) would be longer than that for (20, 8) simply because the rate of release is 4 times smaller. Surprisingly, however, the MWT is only about twice as long, not four times longer (24.6 versus 14.1). In contrast, the MWT for (20, 5) is about threefold larger (41.6 versus 14.1) than the MWT for (20, 8).

These results show that there is no simple relationship between the rate of release I_{SR}, the open time, and the wave velocity. However, the total Ca^{2+} released, $I_{SR} \times T_{open}$, is a fairly good predictor of the SD of the WTD, hence a fairly good predictor of the sharpness of the wave front. Two waves having equal $I_{SR} \times T_{open}$ but different I_{SR}, would appear about equally sharp in linescan images but would have different velocities. In actual linescan images, we do not know $I_{SR} \times T_{open}$, but, because it equals the total Ca^{2+} released, cells with equal $I_{SR} \times T_{open}$ would be about equally bright (compare time plots in Fig. 6, *Ab* and *Cb*). "Equally bright" must be interpreted cautiously, however, when using a nonratiometric dye such as fluo-4.

Initiation of waves

The distinction between wave propagation and wave initiation is essential for understanding the stability of the Ca^{2+} control system in muscle. For ($I_{SR} = 20$, $T_{open} = 5$) the MWT before activating CRUs 2 μm away is 69 $\pm$ 35 ms when the Ca^{2+} distribution is set up using method *a* (Fig. 5 *Ba*, *down triangles*). Because of the large MWT and large SD, we guessed that a wave would not be initiated with these parameters and initial conditions. This guess was, in fact, correct. We carried out a simulation using the same initial conditions as method *a*, firing two columns of seven CRUs that raised the Ca^{2+} concentration locally to high levels, but not enough Ca^{2+} was released to trigger CRU release on adjacent sarcomeres. However, raising the Ca^{2+} concentration to 30 μM in a 4 $\times$ 4 μm region was enough to trigger the wave shown in Fig. 6 *B*.

These examples illustrate the inherent stability of discretely spaced CRUs to even fairly large increases in Ca^{2+} concentration that might arise from injury or the random firing of CRUs. Large enough perturbations can trigger waves, however.

To assess whether a given perturbation, i.e., nonequilibrium Ca^{2+} distribution, can trigger a wave, we calculate the WTD and $P(X \geq 1,\ t < \tau)$ for that perturbation. Fig. 6 *D* shows the WTD for CRU firing at $x = 6$ μm for the standard initial conditions used to start wave calculations, that is, $C(x, y, 0) = 30$ μM on $0 < x < 4$, $0 < y < 4$ (*dashed line*). Note, in this region, that the buffers are in equilibrium with Ca^{2+}, so there is a large reservoir of Ca^{2+}. This WTD has a mean of 18.02 $\pm$ 5.43 ms. Given the short MWT and low SD, we expect that this IC will initiate firing of CRUs at $x = 6$. Initiation does occur and, in Fig. 6 *B,* the CRU at $x = 6$ (3rd spark from the left) fires on schedule at $t = 16$ ms. The reason this perturbation (30 μM on a 4 $\times$ 4 μm^2 region) could initiate a wave but the perturbation of method *a* (two columns of seven firing CRUs) could not is simply related to the amount of Ca^{2+} available to diffuse. In the former case, the large Ca^{2+} reservoir can raise the Ca^{2+} concentration at $x = 6$ μm rapidly and sustain the high concentration; in the latter case, the Ca^{2+} released is rapidly

taken up by buffers, so free Ca^{2+} concentration at $x = 6$ μm is low.

Initiating CRU firing on an adjacent sarcomere does not guarantee wave propagation, however. The Ca^{2+} distribution set up by method *b* serves to assess whether a given set of parameters can support a wave. The WTD using method *b* for ($I_{SR} = 20$, $T_{open} = 5$), which we have seen before, is shown again in Fig. 6 *D (B)*. The large MWT and SD (40.6 ± 30.2 ms) for this WTD make it ambiguous whether a wave might be supported. This ambiguity is reflected in the wave itself as we see in Fig. 6 *B,* where there are times when the wave "stalls" and might seem to cease propagating (e.g., at $x = 12$ μm and 16 μm).

In summary, even if a given set of parameters could support wave propagation, not every disturbance initiates a wave. To initiate a wave, the disturbance must raise the Ca^{2+} concentration sufficiently high over a sufficiently large region. The magnitude and spatial extent of the needed perturbation depends naturally on the parameters and can be estimated from the WTD.

Effect of CRU Ca^{2+} sensitivity

Up to now, we have fixed the CRUs' Ca^{2+} sensitivity K to 15 μM and focused on the effects that I_{SR} and T_{open} have on wave behavior. K is affected by the Mg^{2+} concentration (Rousseau and Meissner, 1989), drugs such as caffeine (Rousseau and Meissner, 1989) and tetracaine (Györke et al., 1997), and SR Ca^{2+} loading (Rousseau and Meissner, 1989; Györke and Györke, 1998). Figure 7 shows the predicted (*curves*) and actual (*open squares*) velocity dependence of v_x on K for $I_{SR} = 20$ pA and $T_{open} = 7$ ms. The lower and upper curves were calculated from the WTD generated using methods *a* and *b*, respectively. The upper and lower boundaries decline almost linearly with K. Similar calculations using $I_{SR} = 10$, $T_{open} = 10$ and $I_{SR} = 20$, $T_{open} = 8$ show also the linear decline of the velocity boundaries, but the slopes differ for each pair of (I_{SR}, T_{open}).

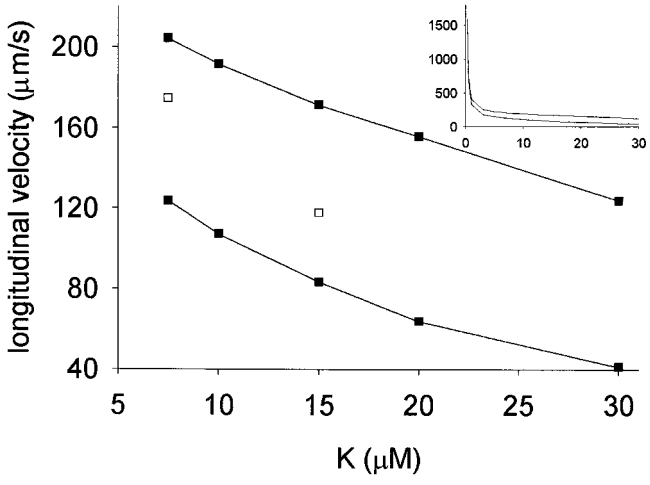

FIGURE 7 Longitudinal velocity dependence on K. Curves give the lower and upper v_x estimates using methods *a* and *b*, respectively. Squares give the actual velocity from wave simulations. Inset shows velocity dependence as K approaches the baseline Ca^{2+} concentration of 100 nM. Computation parameters: $I_{SR} = 20$ pA, $T_{open} = 7$ ms.

Increasing sensitivity and spontaneous waves

Halving K from 15 μM to 7.5 μM doubles the Ca^{2+} sensitivity of the CRU and triples the baseline spark rate, P. Figure 8 shows snapshots of the Ca^{2+} distribution for this high-sensitivity condition. This simulation was started with all chemical species in equilibrium so all sparks arise spontaneously. The first three panels (*left* to *right*) were taken at $t = 21$, 27, and 35 ms, and the arrows point to CRUs at (2, 4), (2, 3.2), and (2, 2.4), respectively. These three contiguous CRUs in the transverse direction fire sequentially and can be seen more clearly in the transverse linescan along $x = 2$ shown in the 12th panel. This sequential firing of sparks in the transverse direction is similar to those observed by Parker et al. (1996) in ventricular cells. Note that not all sparks trigger firing of contiguous CRUs. For example, in panel 2, the spark at (12, 9.6) (near the center) does not trigger any other spark.

Because of the high spontaneous spark rate, it is not surprising to see a wave arise spontaneously. The birth of a wave is seen in panels 4–7. At $t = 45$ ms, the CRU at (16, 9.6) (*panel 4, arrow*) has fired and will sequentially trigger firing of contiguous CRUs on $x = 16$. By $t = 61$ ms (*panel 5*), CRUs at (16, 9.6) and (16, 8.8) have fired and turned off and the CRU at (16, 8) is firing. These sparks on $x = 16$ have raised the Ca^{2+} concentration at (14, 9.6) (*arrow*) only slightly above the baseline, so the firing of the CRU at (14, 9.6) is pure happenstance. If the CRUs on $x = 16$ have not fired, the fate of CRUs on $x = 14$ might be similar to those we have seen: CRU (14, 9.6) might be an isolated spark or it might trigger one or two other sparks.

But the firing of CRUs on $x = 16$ contribute Ca^{2+} to sites on $x = 14$ and also limit the diffusion of Ca^{2+} away from site (14, 9.6). Thus the probability of firing of adjacent CRUs at (14, 9.6 ± 0.8) is slightly higher than the CRU at (2, 3.2) following the CRU (2, 4) firing. Each additional firing of CRUs on $x = 16$ leads to an ever increasing likelihood of CRU firing on $x = 14$ and vice versa, thus stabilizing the nascent wave. After a certain number of CRUs have fired, the probability of the nascent wave dying is virtually zero. This is the probabilistic equivalent of the "critical curvature" a wave must have before it can propagate (Wussling et al., 1997).

Effect of transverse lattice spacing

What effect would reducing the transverse CRU spacing from $\ell_y = 0.8$ to 0.4 μm, keeping ℓ_x fixed to 2 μm, have on

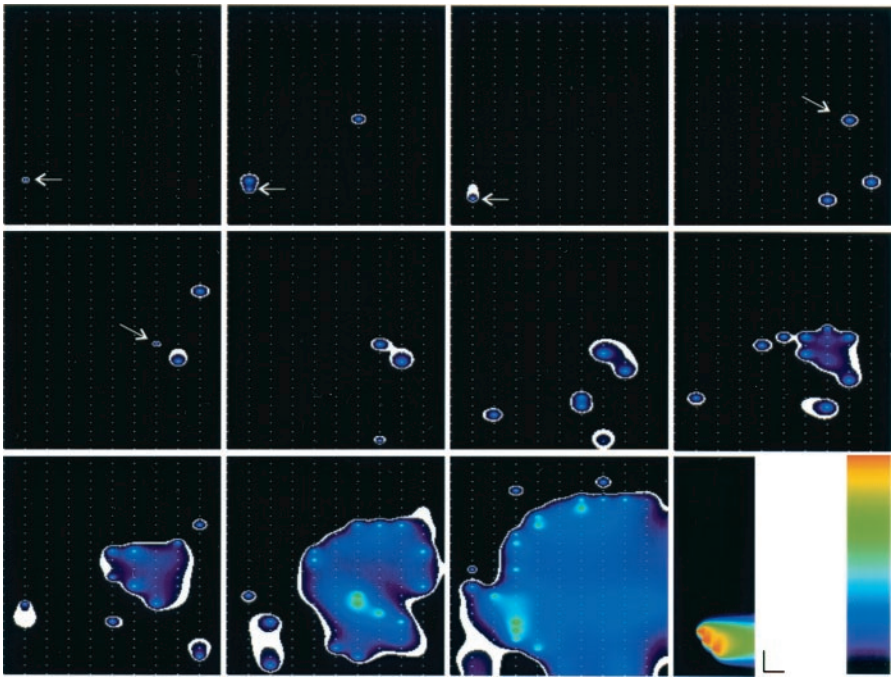

FIGURE 8 High Ca^{2+} sensitivity (K) causes spontaneous wave. Snapshots of Ca^{2+} distribution at 21, 27, 35, 45, 61, 65, 72, 80, 90, 110, and 130 ms showing the spontaneous appearance of a Ca^{2+} wave. K is 7.5 μM, twice the usual sensitivity, giving rise to numerous spontaneous sparks. The first three panels show the sequential firing of three CRUs at $x = 2$ (*arrows*). A transverse linescan showing the dye concentration (time flowing from left to right) at $x = 2$ is in panel 12. Although there are numerous spontaneous sparks, most do not trigger a wave. The birth of the wave is seen in panels 5–7. The wave starts from spontaneous sparks on adjacent sarcomeres ($x = 14$ and 16) occurring at about the same time at about the same y value (~8). Scale bar 20 ms and 2 μm, color bar ranges from 0.1 to 350 μM for Ca^{2+} and 4 to 50 μM for the Ca-bound dye. Computation parameters: $I_{SR} = 20$ pA, $T_{open} = 7$ ms, $K = 7.5$ μM.

the ratio of ν_x to ν_y? When $\ell_y = 0.8$ μm, $\nu_x/\nu_y \approx 1.3$; for the wave in Fig. 4, $\nu_x/\nu_y = 155$ μm/s/124 μm/s = 1.25. When ℓ_y is reduced to 0.4 μm, the distance to the adjacent CRU in the y-direction is only ⅕ of that to the CRU on the next sarcomere. Thus the shorter distance should compensate for the 2:1 diffusion anisotropy, and we might expect ν_x/ν_y to be less than unity. This expectation is wrong.

Figure 9 shows snapshots of a Ca^{2+} wave propagating on a lattice with $\ell_x = 2$ μm and $\ell_y = 0.4$ μm at 37-ms time intervals starting at $t = 0$ ms. As in Fig. 4, the white dots mark the CRU locations and the white curve shows where 10 μM $< C <$ 20 μM. Contrary to our naive expectation, the longitudinal velocity is almost twice as large as the transverse velocity, 120 μm/s versus 67 μm/s. In this simulation $I_{SR} = 15$, $T_{open} = 6$, and $K = 15$ μM. Simulations using (I_{SR}, T_{open}) = (10, 10) or (10, 16) gave ν_x/ν_y ratios of 1.7. Thus the change in ellipticity of the Ca^{2+} wave went opposite to our expectation.

This surprising behavior has its origin in the way waves propagate on discrete lattices that we outlined earlier. Recall that, in Fig. 4, about 5–7 contiguous CRUs along a column (i.e., z-line) were needed to fire to sufficiently saturate the buffers and raise the Ca^{2+} concentration enough to trigger firing at the next sarcomere. Thus the rate at which the wave progressed along the x-direction was intimately linked to the rate CRUs along the y-direction were triggered. When $\ell_y = 0.4$ μm the rate the CRUs along y are activated is faster than when $\ell_y = 0.8$ (for the same parameters), but then, so are the CRUs on adjacent sarcomeres. Thus we do not get an elliptically shaped wave with major axis in the y-direction.

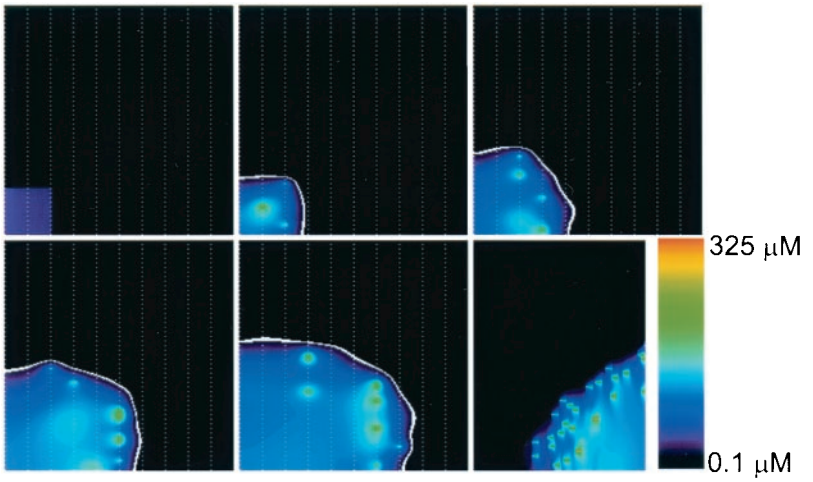

FIGURE 9 Effect of transverse lattice spacing on wave propagation. The transverse spacing of CRUs has been reduced from 0.8 to 0.4 μm. The naive expectation that the wave will travel faster transversely than longitudinally when ℓ_y is reduced is not borne out as shown in these Ca^{2+} concentration images. The longitudinal velocity is about twice as large as the transverse velocity (~120 μm/s versus ~67 μm/s). These images were taken at 37-ms intervals starting at $t = 0$. The longitudinal spacing of CRUs is 2 μm as usual. The sixth image is the transverse linescan at $x = 6$ μm shows the rapid activation of ~15 CRUs (flat part of the linescan) followed by slower activation further for larger y; this behavior is similar to that in Fig. 4. Computation parameters: $I_{SR} = 15$ pA, $T_{open} = 6$ ms, $K = 15$ μM.

The transverse linescan (*image 6*), taken at $x = 6$ μm, shows the rapid activation of ~15 CRUs along the y-direction indicated by the flat apex.

DISCUSSION

Based on newly available information on excitation–contraction coupling, we developed and analyzed a mathematical model that provides a unified framework for understanding the relationship between Ca^{2+} sparks and Ca^{2+} waves. The key elements of this model include the use of relatively large currents to generate Ca^{2+} sparks, stochastic triggering of SR Ca^{2+} release, asymmetric distribution of CRUs, and the anisotropic diffusion of Ca^{2+} and mobile buffers. Significantly, Ca^{2+} waves produced by our model mimic the important features of Ca^{2+} waves in experiments in terms of velocity, pattern of propagation (anisotropy), and changes in the spontaneous Ca^{2+} spark frequency. Also, our model is unique in its ability to reproduce these features using experimentally measured parameter values.

Importance of using large currents

In our initial efforts to model Ca^{2+} waves (Izu et al., 1999), we assumed that the current through the CRU was ~1–2 pA. These small currents generated unrealistic waves that traveled along the transverse direction where the CRU spacing was 0.8 μm, but not along the longitudinal direction because the CRU spacing was 2 μm. Moreover, to get waves to propagate even in the transverse direction, the CRU Ca^{2+} sensitivity had to be set to $K \approx 500$ nM, about 30-fold smaller than measured in planar bilayer studies (Györke and Györke, 1998) and in permeabilized cells (Lukyanenko and Györke, 1999).

The failure of the model to generate realistic waves forced us to reexamine our basic understanding of Ca^{2+} sparks (Izu et al., 2001), where we estimated that the current underlying a spark is about 20 pA, about 10 times larger than the prevailing estimate. Ríos et al. (1999), using different methods, estimated that the currents underlying sparks in skeletal muscle are between 15 and 20 pA.

In this paper, we used CRU currents between 10 and 20 pA. With currents of this magnitude, the Ca^{2+} waves appear realistic, propagating faster longitudinally than transversely ($\nu_x/\nu_y \approx 1.3$–1.7) despite the longer distance between CRUs along x ($\ell_x = 2$ μm) than y ($\ell_y = 0.4$–0.8 μm). Such velocity anisotropy is observed in cardiac cells where ν_x/ν_y ranges from 1.30 at 17°C to 1.55 at 37°C (Engel et al., 1994).

Importantly, realistic waves are obtained using Ca^{2+} sensitivity values of $K \sim 15$ μM, which is in the range measured in planar bilayers (Györke and Györke, 1998) and permeabilized cells (Lukyanenko and Györke, 1999) with physiological levels of Mg^{2+}. In an earlier model for Ca^{2+} waves (Keizer and Smith, 1998), where release fluxes corresponding to currents of ~2 pA were used, K_e, which roughly corresponds to the Ca^{2+} sensitivity, had to be reduced 5000-fold to achieve "stochastic excitability" at a Ca^{2+} concentration of 100 nM. Keizer and Smith also used a maximum pump rate of 2 μM/s, which is 100 times smaller than the experimentally measured value (Balke et al., 1994). The small maximum pump rate might have been necessary to allow wave propagation in their model.

Lukyanenko et al. (1999), using a derivative of the Keizer and Smith model, also found that, for wave propagation to occur when CRUs were separated by 2 μm, the threshold for release had to be set to low (<1.5 μM) levels.

Although we do not use a release flux (units of μM/s) but a molar flux (pmol/μm/ms), it is of interest to compute a release flux from our model parameters to compare with values determined by others. As described in Methods, we assumed 1 CRU/z-line and use a volume commensurate with the confocal scan region (1 μm × 0.5 μm) and sarcomere length (2 μm). Thus we assume 2 CRU/μm^3. Assuming each CRU carries 20 pA, then the release flux equals 200 μM/ms. This value is ~30–100 times larger than previous estimates for a cardiac spark (Blatter et al., 1997; Lukyanenko et al., 1998). Our release flux value is, however, fairly close to the ~350 μM/ms recently calculated by Ríos et al. (1999). It is hard to reconcile Ca^{2+} wave propagation with CRUs having relatively low Ca^{2+} sensitivity of ~15 μM when using the earlier release flux estimates of ~2–7 μM/ms.

Constraints imposed by stochastic models

Because spontaneous sparks appear to be the product of random opening and closing of RyRs, models linking sparks to waves must have stochastic control of the opening and closing of RyRs. This is important because deterministic and stochastic systems can behave very differently when the Ca^{2+} sensitivity of the CRUs (K) is high. In particular, in a deterministic system, the baseline Ca^{2+} concentration (C_0) can be brought arbitrarily close to the firing threshold without triggering a wave. In our stochastic model, if K is reduced to near C_0, then the number of spontaneous sparks increases rapidly. In Fig. 8, we see numerous spontaneous sparks that coalesce into a wave even when $K = 7.5$ μM $\gg$ $C_0 = 0.1$ μM. If $K \approx C_0$, the spontaneous spark rate would be so high (up to P_{max}) that the multitude of spontaneous sparks would be like raindrops on a pond precluding an organized wave, i.e., one starting at one end of the cell that progresses to the other end. It is likely that if Lukyanenko et al. (1999) had used a stochastic instead of a deterministic model for triggering Ca^{2+} release, then, for the threshold used that allowed wave propagation (<1.5 μM), the number of spontaneous sparks would be so large that well organized waves would not have formed.

Thus stochastic systems imposes the constraint $K \gg C_0$ for organized waves to occur. This constraint is important when we consider factors that affect wave velocity.

Determinants of wave velocity

The wave velocity is affected by the rate of Ca^{2+} release, I_{SR}, the total amount of Ca^{2+} released, $I_{SR} \times T_{open}$, and the Ca^{2+} sensitivity of the CRU, K. The Ca^{2+} sensitivity of RyRs is affected by the Mg^{2+} concentration (Rousseau and Meissner, 1989; Györke and Györke, 1998), SR loading (Györke and Györke, 1998), and drugs such as caffeine (Rousseau and Meissner, 1989) and tetracaine (Györke et al., 1997). Figure 7 shows the estimated dependence of the longitudinal wave velocity ν_x on K. As expected, increasing the Ca^{2+} sensitivity (decreasing K) increases the wave velocity. In fact, such a velocity increase has been observed in the presence of low doses of caffeine (Lukyanenko et al., 1999).

The main graph of Fig. 7 shows the estimated bounds of ν_x declining roughly linearly with K. However, the inset shows that, as K decreases to near C_0 (0.1 μM) the wave velocity rises sharply; for $K = 0.3$ μM, the estimated velocity $\approx$ 1600 μm/s. ter Keurs and co-workers (Miura et al., 1999) have measured very high velocity ($\sim$1000–2000 μm/s) Ca^{2+} waves in intact trabeculae that increased (to $\sim$6000 μm/s) in the presence of caffeine. They ascribe the changes in velocity to changes in cellular loading and open probability of CRUs. The sharp rise of ν_x as $K \rightarrow C_0$ would be in accord with their explanation, but we find it a challenge to explain such high wave velocities within the context of our stochastic model because the number of spontaneous sparks would be so great that no well-organized wave would emerge.

An unexpected finding of this study was that the "local" wave velocity was strongly affected by the total Ca^{2+} released, $I_{SR} \times T_{open}$. The local or instantaneous wave velocity is the distance between two CRUs ($\ell_x = 2$ μm) divided by the time interval between their firing. Large variations in the local wave velocity are seen as a ragged wave front in linescan images (Fig. 6 *B)* and were also noted by Cheng et al. (1996) in rat ventricular myocytes. Large variations in the wave speed reflect the broad waiting-time distribution that arises when total Ca^{2+} released is low ($I_{SR} \times T_{open} = 20$ pA $\times$ 5 ms = 100 fC) Fig. 6 *D, curve B).*

Figure 6, *A* and *C,* show two waves having different velocities because the underlying currents are different (20 pA and 5 pA) yet their wave fronts are about equally sharp because T_{open} was adjusted to make $I_{SR} \times T_{open}$ equal in both cases (160 fC). The waiting time distribution curves (Fig. 6 *D, curves A* and *C)* are shifted because of the different currents but roughly similar standard deviations. The two images are of about equal brightness because the total Ca^{2+} released are the same. Acknowledging the perils of comparing fluo-4 image brightness, we suggest, as a rule-of-thumb, that wave images of comparable brightness will have wave fronts of comparable sharpness. In particular, bright waves will have sharp wave fronts, and dim waves will have ragged fronts.

Controlling instability

The paradox of stable cytosolic Ca^{2+} levels in the face of regenerative SR Ca^{2+} release has been largely resolved by Stern's (1992) local control model of Ca^{2+} release and confirmed experimentally with the discovery of Ca^{2+} sparks (Cheng et al., 1993). Anatomy (in part) confers stability: stability is achieved by the separation of CRUs by about 2 μm longitudinally and about 0.4–0.8 μm in the plane of the z-line. Ca^{2+} buffers severely restrict the spread of Ca^{2+} released from a single or few CRUs, where superadditivity effects are minimal, as seen in Fig. 2. Even for large currents ($\sim$20 pA), the maximum Ca^{2+} concentration 2 μm away from a CRU (in the x direction) is less than 300 nM. However, CRUs are spaced more closely in the transverse direction and the Ca^{2+} concentration at the CRU adjacent to the one that is firing 0.8 μm away can be high. For example, for a CRU with $I_{SR} = 20$ pA and $T_{open} = 7$ ms, the Ca^{2+} concentration 0.8 μm away is 2.9 μM. However, because $K \sim 15$ μM, the probability that a neighboring CRU will fire within 150 ms is 0.38. Note that, if the CRU spacing is assumed to be 0.4 μm, the probability of triggering a neighbor within 150 ms increases only to 0.42 because $\bar{P}$ is less. Stability is also enhanced slightly by the anisotropy favoring diffusion along x over y. If diffusion were isotropic then the probability of triggering a neighbor within 150 ms rises to 0.52. Thus stability derives from spatial separation of CRUs, low Ca^{2+} sensitivity of the CRUs, Ca^{2+} buffering, and, to a lesser extent, diffusional anisotropy.

Loss of stability can manifest itself in Ca^{2+} waves. Because increased SR loading increases both I_{SR} (measured by the spark amplitude, Cheng et al., 1996; Satoh et al., 1997) and CRU Ca^{2+} sensitivity (decreases K), it is not surprising that increasing SR load is perhaps the most common way of inducing spontaneous waves. As seen in Fig. 8, reducing K to 7.5 μM caused a spontaneous wave. However, we also see that not every spontaneous spark generates a wave. Precisely how many sparks in what configuration is needed to start a wave is difficult if not impossible to predict. The simulation in Fig. 8 suggests, however, that 2 sparks on adjacent z-lines within about 1 lattice step in the y-direction, firing within a few milliseconds of each other is sufficient to trigger a wave. The reason why this configuration can trigger a wave is due, in part, from the shallow concentration gradient between the releasing sites along x that forces more Ca^{2+} to flow in the y-direction and activate transverse neighbors. Each additional firing of CRUs on one z-line leads to an ever increasing likelihood of CRU firing on the other z-line and vice versa. Soon, transverse CRUs on the

neighboring z-lines begin to fire sequentially in lockstep, generating a stable nascent wave. After a certain number of CRUs have fired, the probability of the nascent wave dying spontaneously becomes virtually zero. The minimal spark configuration that can initiate a stable wave is equivalent to the critical curvature a wave must have before it can propagate (Wussling et al., 1997).

In ventricular cells, Ca^{2+} waves are believed to be a pathological manifestation of Ca^{2+} overload. However, in other cell types such as avian ventricular cells or atrial cells that do not have t-tubules, Ca^{2+} waves might assume the function of t-tubules in causing rapid, propagated Ca^{2+} release throughout the cell. In these cells it would be important for a state of "controlled instability" to be maintained, wherein random Ca^{2+} fluctuations would not trigger a wave but a large enough Ca^{2+} bolus, representing a useful signal, would start a wave.

Limitations of the model

One problem is the very slow decline of the Ca^{2+} wave. In our longest simulation of 300 ms, the Ca-bound dye concentration ([Ca-Dye]) had not declined to the baseline level. We estimate from the maximum pump rate of 200 μM/s and the amount of Ca^{2+} released that it would take ~2000 ms for [Ca-Dye] to return to baseline. Lukyanenko et al. (1998) had used a maximum pump rate 10 times larger than ours, and, using this rate, we calculated that the wave would decline in about 200 ms.

The slow decline might be due, in part, to the absence of diffusion in the z-direction because of cylindrical symmetry. We partially compensated for this by reducing the molar flux (see Methods). This suggests that the too slow decline of the wave might be linked to another limitation of the model—representing the cell as a 2D plane. At the moment, computational limitations preclude a full 3D simulation. However, a 2D simulation might not be as inaccurate as it might first appear. Rapid 3D confocal imaging of Ca^{2+} waves using a novel Nipkow confocal microscope (Ishida et al., 1999) shows that there is little variation of the wave in the z-direction. This amounts to cylindrical symmetry assumed in our 2D model. Thus a 3D simulation would require CRUs to fire throughout the y–z plane, so would not solve the problem of the slowly declining wave.

Another limitation of the model is that T_{open} is fixed for all CRUs in a particular simulation. We have seen that wave properties are particularly sensitive to T_{open}. Even a 1-ms change can substantially affect the MWT and SD of the waiting time distribution. In future work we will allow T_{open} to be a random variable.

As mentioned in Methods, we used the Smith buffer model (Smith et al., 1998) instead of the more complex Harkins buffer model (Harkins et al., 1993) because the computational burden of using the latter was prohibitive. To get a sense of how using the Harkins model would affect wave propagation, we compared the Ca^{2+} concentrations from the two models at various distances away from a point source (assuming spherical symmetry, see Izu et al., 2001). In the Harkins model, protein-bound fluo-3 (PD) can bind Ca^{2+} and also act as a large reservoir for protein-free fluo-3 (D), which has a higher Ca^{2+} affinity than PD. Thus for the same concentration of D in the Smith and Harkins buffer models, there are more Ca^{2+} binding sites in the Harkins buffer model resulting in a lower maximum Ca^{2+} concentration for the same current. The magnitude of the difference depends on the distance from the source, r, however. For both Smith and Harkins buffer models C at $r = 0.4$ μm are almost identical and the probability of triggering a CRU at this distance is almost 1 within 15 ms. These calculations used $I_{SR} = 40$ pA, $T_{open} = 5$ ms, $D_{Cx} = 0.3$ μm^2/ms, $D_{Dx} = 0.09$ μm^2/ms (for Harkins model) or $D_{Dx} = 0.02$ μm^2/ms (for Smith model). These currents are much larger than used in the 2D simulations because spherical symmetry is assumed. See Izu et al. (2001) on the effect of symmetry assumptions. At $r = 2$ μm, C rises to ~160 nM and ~140 nM in the Smith and Harkins models, respectively. Offsetting the smaller maximum Ca^{2+} concentration is the faster rise time in the Harkins model, so, within ~50 ms of firing of the source CRU, the probability of triggering a CRU at $r = 2$ is about the same for both models.

Given these compensating effects in the Harkins model, we cannot make quantitative predictions of Ca^{2+} wave properties in the Harkins model without simulations. We would guess, however, that the wave velocity would be slower and it would be more difficult to initiate a wave because there is effectively more exogenous buffer than in the Smith model.

Insufficient computational power imposes many of the limits of the model. The most important are the limitation to 2D simulations and the use of a simple Ca^{2+} buffer model. We are currently writing simulation code to run on a supercomputer (an SGI Origin 2000) that would remove these limitations. Supercomputer calculations will also allow much longer simulation times ($\gg$ 150 ms) allowing us to study Ca^{2+} oscillations. Currently, we prevent CRU refiring (hence oscillations) by setting the refractory period to virtual infinity to avoid complicating the analysis of propagation of a single Ca^{2+} wave.

The use of a stochastic function that depends algebraically on the local Ca^{2+} concentration (i.e., changing instantly with C), instead of being a dynamical function, is both a strength and a weakness. Its simplicity allowed us to calculate probability functions that were extremely useful for guiding the simulations and provided insights into the factors that control wave propagation. However, its utter simplicity might be preventing us from seeing waves that are self-aborting, as Keizer and Smith (1998) observed in their simulations. (There are trivially self-aborting waves that exist for a short time because of high Ca^{2+} concentra-

tions that are put in as initial conditions.) In our model, after a wave gets beyond a certain size, it never dies.

In summary, the model presented here provides a unified framework for studying both Ca^{2+} sparks and Ca^{2+} waves in cardiac ventricular myocytes. The model generates spontaneous Ca^{2+} sparks at rates seen in experiments. The model also generates realistic Ca^{2+} waves using relatively low ($\sim$15 μM) Ca^{2+} sensitivities for the SR Ca^{2+} release units.

APPENDIX A

It can be readily verified that the solution to the linear 2D anisotropic diffusion problem,

$$\frac{\partial C}{\partial t} = D_x \frac{\partial^2 C}{\partial x^2} + D_y \frac{\partial^2 C}{\partial y^2}, \tag{A1}$$

satisfying the boundary condition $u(x, y, t) \to 0$ as $x, y \to \infty$ and initial condition $C(x, y, 0) = M\delta(x, y)$ is

$$C(x, y, t) = \frac{M}{4\pi\sqrt{D_x D_y}t} \exp\left(\frac{-x^2}{4D_x t}\right) \cdot \exp\left(\frac{-y^2}{4D_y t}\right) \equiv MG(x, y, t), \tag{A2}$$

where G is the Green's function. We model the opening of the CRU with a source $\psi(t)$ that has constant value q between $0 < t < T$ and is zero otherwise,

$$\psi(t) = qH(t) - qH(t - T), \tag{A3}$$

where H is the Heaviside function. The Ca^{2+} distribution in this case is found by convolving the Green's function with ψ. The convolution with the first term is

$$\int_0^t qG(x, y, t - s)H(s)\,ds = \frac{q}{4\pi\sqrt{D_x D_y}} \int_{\gamma/(4t)}^{\infty} \frac{e^{-z}}{z}\,dz = \frac{q}{4\pi\sqrt{D_x D_y}} E_1\left(\frac{\gamma}{4t}\right), \tag{A4}$$

where $\gamma = (x^2 D_y + y^2 D_x)/(D_x D_y)$, $z = \gamma/[4(t - s)]$, and E_1 is the exponential integral. The convolution of the second term of ψ with G is obtained similarly, and $C(x, y, t)$ becomes

$$C(x, y, t) = \frac{q}{4\pi\sqrt{D_x D_y}} \left[E_1\left(\frac{\gamma}{4t}\right)H(t) - E_1\left(\frac{\gamma}{4(t - T)}\right)H(t - T)\right] \equiv \frac{q}{4\pi\sqrt{D_x D_y}} \tilde{E}_1(x, y, t, T), \tag{A5}$$

where we call $\tilde{E}$ the "extended exponential integral."

APPENDIX B

We derive the probability that a CRU at (x, y) will not fire in $t < \tau$, $p(t < \tau)$, and the waiting time distribution, $\varphi(\tau)$, when the probability of occurrence per unit time $P(C(x, y, t), K, n)$ varies with time. When P is constant and $\ll 1$, then the waiting time distribution is the exponential distribution (see any textbook on probability, e.g., Ross, 1976). We are unaware of a derivation for φ when P is variable.

The probability that we need to wait at least time τ before the channel opens equals 1 − (probability that no event occurred in $t < \tau$). Divide τ up into δt time segments, $\tau = N\delta t$, then the probability that no event occurred is

$$p(t < \tau) = (1 - P(t_1)\delta t(1 - P(t_2)\delta t) \cdots (1 - P(t_N)\delta t), \tag{B1}$$

where we use the abbreviated notation $P(t_i) = P(C(x, y, t_i), K, n)$ and $(i - 1)\delta t \le t_i \le i\,\delta t$. Taking logs

$$\ln(p(t < \tau)) = \sum_i \ln(1 - P(i)\delta t) \approx -\sum_i P(i)\delta t. \tag{B2}$$

The approximation holds provided $P(i) \ll 1$, which means that $C(x, y, t)$ should be much smaller than K. Letting $\delta t \to 0$, gives the key result,

$$p(t < \tau) = \exp\left(-\int_0^\tau P(s)\,ds\right). \tag{B3}$$

The probability that one has to wait at least τ for an event to occur is $p(t > \tau) = 1 - p(t < \tau)$. The waiting time distribution φ that generates $p(t > \tau)$ is defined by

$$p(t > \tau) = \int_{-\infty}^{\tau} \varphi(s)\,ds. \tag{B4}$$

Differentiating with respect to τ gives

$$\varphi(x, y, \tau) = \begin{cases} P(C(x, y, \tau))\exp\left(-\int_0^\tau P(C(x, y, s)\,ds)\right) & \tau > 0 \\ 0, & \tau \le 0. \end{cases} \tag{B5}$$

The mean waiting time $\bar{\tau}$ is

$$\bar{\tau} = \int_0^\infty \tau\varphi(x, y, \tau)\,d\tau. \tag{B6}$$

Note that, if $P(C(x, y, t), K, n) = \bar{P}$ is constant, then the mean waiting time reduces to the well-known solution $\bar{\tau} = 1/\bar{P}$.

Waiting time distribution for *N* CRUs.

If $p_i(t < \tau)$ is the probability that the ith CRU has not fired in $t < \tau$, then the probability of having to wait at least time τ before at least one of the N CRUs have fired is

$$P(X \ge 1, t < \tau) = 1 - \prod_{i=1}^{N} p_i = 1 - \prod_{i=1}^{N} \exp\left(-\int_0^\tau P(C(x_i, y_i, s)\,ds)\right). \tag{B7}$$

Differentiating with respect to τ gives

$$\varphi(\tau) = \begin{cases} \left(\sum_i P(C(x_i, y_i, \tau)) \right) \cdot \prod_i p_i(t < \tau), & \tau > 0 \\ 0, & \tau \le 0. \end{cases} \quad \text{(B8)}$$

We thank Ye Chen-Izu (University of Maryland) and Robert A. Spangler (State University of New York at Buffalo) for valuable discussions. L.T.I. was supported by National Institutes of Health/National Institute of Arthritis and Musculoskeletal and Skin Diseases Institutional Training Grant AR07592 to the Interdisciplinary Program in Muscle Biology, University of Maryland School of Medicine.

REFERENCES

Backx, P. H., P. P. De Tombe, J. H. K. Van Deen, B. J. M. Mulder, and H. E. D. J. ter Keurs. 1989. A model of propagating calcium-induced calcium release mediated by calcium diffusion. *J. Gen. Physiol.* 93: 963–977.

Balke, C. W., T. M. Egan, and W. G. Wier. 1994. Processes that remove calcium from the cytoplasm during excitation–contraction coupling in intact rat heart cells. *J. Physiol.* 474:447–462.

Blatter, L. A., J. Hüser, and E. Ríos. 1997. Sarcoplasmic reticulum Ca^{2+} release flux underlying Ca^{2+} sparks in cardiac muscle. *Proc. Natl. Acad. Sci. USA.* 94:4176–4181.

Bugrim, A. E., A. M. Zhabotinsky, and I. R. Epstein. 1997. Calcium waves in a model with a random spatially discrete distribution of Ca^{2+} release sites. *Biophys. J.* 73:2897–2906.

Carl, L. S., K. Felix, A. H. Caswell, N. R. Brandt, W. J. Ball, Jr., P. L. Vaghy, G. Meissner, and D. G. Ferguson. 1995. Immunolocalization of sarcolemmal dihydropyridine receptor and sarcoplasmic reticular triadin and ryanodine receptor in rabbit ventricle and atrium. *J. Cell Biol.* 129:673–682.

Cheng, H., M. R. Lederer, W. J. Lederer, and M. B. Cannell. 1996. Calcium sparks and $[Ca^{2+}]_i$ waves in cardiac myocytes. *Am. J. Physiol. Cell Physiol.* 270:C148–C159.

Cheng, H., W. J. Lederer, and M. B. Cannell. 1993. Calcium sparks: elementary events underlying excitation–contraction coupling in heart muscle. *Science.* 262:740–744.

Cornell-Bell, A. H., and S. M. Finkbeiner. 1991. Ca^{2+} waves in astrocytes. *Cell Calcium.* 12:185–204.

Endo, M., M. Tanaka, and Y. Ogawa. 1970. Calcium induced release of calcium from the sarcoplasmic reticulum of skinned skeletal muscle fibers. *Nature.* 228:34–36.

Engel, J., M. Fechner, A. J. Sowerby, S. A. E. Finch, and A. Stier. 1994. Anisotropic propagation of Ca^{2+} waves in isolated cardiomyocytes. *Biophys. J.* 66:1756–1762.

Fabiato, A., and F. Fabiato. 1972. Excitation–contraction coupling of isolated cardiac fibers with disrupted or closed sarcomeres. Calcium-dependent cyclic and tonic contractions. *Circ. Res.* 31:293–307.

Ford, L. E., and R. J. Podolsky. 1970. Regenerative calcium release within muscle cells. *Science.* 167:58–59.

Girard, S., A. Luckhoff, J. Lechleiter, J. Sneyd, and D. Clapham. 1992. Two-dimensional model of calcium waves reproduces the patterns observed in *Xenopus* oocytes. *Biophys. J.* 61:509–517.

Györke, S., and I. Györke. 1998. Regulation of the cardiac ryanodine receptor channel by luminal Ca^{2+} involves luminal Ca^{2+} sensing sites. *Biophys. J.* 75:2801–2810.

Györke, S., V. Lukyanenko, and I. Györke. 1997. Dual effects of tetracaine on spontaneous calcium release in rat ventricular myocytes. *J. Physiol.* 500:297–309.

Harkins, A. B., N. Kurebayashi, and S. M. Baylor. 1993. Resting myoplasmic free calcium in frog skeletal muscle fibers estimated with fluo-3. *Biophys. J.* 65:865–881.

Hüser, J., S. L. Lipsius, and L. A. Blatter. 1996. Calcium gradients during excitation–contraction coupling in cat atrial myocytes. *J. Physiol.* 494: 641–651.

Ishida, H., C. Genka, Y. Hirota, H. Nakazawa, and W. H. Barry. 1999. Formation of planar and spiral Ca^{2+} waves in isolated cardiac myocytes. *Biophys. J.* 77:2114–2122.

Izu, L. T., J. R. H. Mauban, C. W. Balke, and W. G. Wier. 2001. Large currents generate cardiac Ca^{2+} sparks. *Biophys. J.* 80:88–102.

Izu, L. T., W. G. Wier, and C. W. Balke. 1999. Evolution of Ca^{2+} waves from stochastic Ca^{2+} sparks on rectangular lattices. *Biophys. J.* 76: A397.

Jiang, Y.-H., M. G. Klein, and M. F. Schneider. 1999. Numerical simulation of Ca^{2+} "sparks" in skeletal muscle. *Biophys. J.* 77:2333–2357.

Kargacin, G., and F. S. Fay. 1991. Ca^{2+} movement in smooth muscle cells studied with one- and two-dimensional diffusion models. *Biophys. J.* 60:1088–1100.

Keizer, J. and G. D. Smith. 1998. Spark-to-wave transition: saltatory transmission of calcium waves in cardiac myocytes. *Biophys. Chem.* 72: 87–100.

Keizer, J., G. D. Smith, S. Ponce-Dawson, and J. E. Pearson. 1998. Saltatory propagation of Ca^{2+} waves by Ca^{2+} sparks. *Biophys. J.* 75: 595–600.

Lakatta, E. G., and T. Guarnieri. 1993. Spontaneous myocardial calcium oscillations: are they linked to ventricular fibrillation? *J. Cardiovasc. Electrophysiol.* 4:473–489.

Lukyanenko, V., and S. Györke. 1999. Ca^{2+} sparks and Ca^{2+} waves in saponin-permeabilized rat ventricular myocytes. *J. Physiol.* 521: 575–585.

Lukyanenko, V., S. Subramanian, I. Györke, T. F. Wiesner, and S. Györke. 1999. The role of luminal Ca^{2+} in the generation of Ca^{2+} waves in rat ventricular myocytes. *J. Physiol.* 518:173–186.

Lukyanenko, V., T. F. Wiesner, and S. Györke. 1998. Termination of Ca^{2+} release during Ca^{2+} sparks in rat ventricular myocytes. *J. Physiol.* 507:667–677.

Miura, M., P. A. Boyden, and H. E. D. J. ter Keurs. 1999. Ca^{2+} waves during triggered propagated contractions in intact trabeculae. Determinants of the velocity of propagation. *Circ. Res.* 84:1459–1468.

Parker, I., W.-J. Zang, and W. G. Wier. 1996. Ca^{2+} sparks involving multiple Ca^{2+} release sites along *z*-lines in rat heart cells. *J. Physiol.* 497:31–38.

Ridgway, E. B., J. C. Gilkey, and L. F. Jaffe. 1977. Free calcium increases explosively in activating medaka eggs. *Proc. Natl. Acad. Sci. USA.* 74:623–627.

Ríos, E., M. D. Stern, A. González, G. Pizzarro, and N. Shirokova. 1999. Calcium release flux underlying Ca^{2+} sparks of frog skeletal muscle. *J. Gen. Physiol.* 114:31–48.

Ross, S. 1976. A first course in probability. Macmillan, New York.

Rousseau, E., and G. Meissner. 1989. Single cardiac sarcoplasmic reticulum Ca^{2+}-release channel: activation by caffeine. *Am. J. Physiol. Heart Circ. Physiol.* 256:H328–H333.

Satoh, H., L. A. Blatter, and D. M. Bers. 1997. Effects of $[Ca^{2+}]_i$, SR Ca^{2+} load, and rest on Ca^{2+} spark frequency in ventricular myocytes. *Am. J. Physiol. Heart Circ. Physiol.* 272:H657–H668.

Shacklock, P. S., W. G. Wier, and C. W. Balke. 1995. Local Ca^{2+} transients (Ca^{2+} sparks) originate at transverse tubules in rat heart cells. *J. Physiol.* 487:601–608.

Smith, G. D., J. E. Keizer, M. D. Stern, W. J. Lederer, and H. Cheng. 1998. A simple numerical model of calcium spark formation and detection in cardiac myocytes. *Biophys. J.* 75:15–32.

Stern, M. D. 1992. Theory of excitation–contraction coupling in cardiac muscle. *Biophys. J.* 63:497–517.

Wussling, M. H., K. Scheufler, S. Schmerling, and V. Drygalla. 1997. Velocity–curvature relationship of colliding spherical calcium waves in rat cardiac myocytes. *Biophys. J.* 73:1232–1242.